

Proximal DCA for Fréchet Regression on Riemannian Manifolds with Bounded Curvature*

Yamin Zhou César A. Uribe

Department of Electrical and Computer Engineering and Ken Kennedy Institute
Rice University, Houston, TX

yz282@rice.edu cauribe@rice.edu

Abstract

Fréchet regression generalizes linear regression to metric-space-valued responses by defining fitted values as minimizers of weighted Fréchet functionals. Since these weights may have mixed signs, the resulting objective is a signed barycenter problem rather than a standard convex barycenter problem. On Riemannian manifolds, this is further complicated by the lack of global geodesic convexity and possible nonsmoothness of squared distances near cut loci. We study signed Fréchet regression on complete manifolds with two-sided bounded sectional curvature. By restricting optimization to a strongly convex normal ball containing the response support, we use local smoothness, Hessian comparison, and Jacobi-field estimates to formulate the problem as a locally controlled Riemannian proximal DC problem. This leads to FRIDA (Fréchet Regression via Riemannian Iterative DC Algorithm), an exact and inexact proximal DC algorithm for computing regression fits. We prove existence and interiority of minimizers under explicit signed-weight conditions, establish curvature-dependent strong convexity of the proximal subproblems, and show descent and convergence of the iterates to stationary points. We also derive sublinear complexity estimates and, under real-analyticity, obtain full-sequence convergence with KL-type local rates. These results provide a rigorous optimization framework for signed Fréchet regression on manifolds with bounded curvature.

1 Introduction

Fréchet regression extends classical regression to metric-space-valued responses by defining fitted values through weighted Fréchet minimization. The global model of Petersen and Müller [22] gives a conditional Fréchet mean at each query point x , and has motivated extensions to network-valued responses, total-variation regularization, manifold-valued curve regression, and non-Euclidean predictors [12, 19, 21, 25, 32]. Most existing work emphasizes statistical theory, such as consistency, convergence rates, and model extensions, while the computation of Fréchet regression fits remain comparatively underdeveloped, especially on curved response spaces where the objective is not geodesically convex.

A key feature of global Fréchet regression is that its weights may have mixed signs. Given observations $\{(x_i, y_i)\}_{i=1}^m$, the fitted value at a query point $x \in \mathbb{R}^q$ is obtained from

$$\min_{y \in \mathcal{M}_{\text{ex}}} f(y, x) \triangleq \sum_{i=1}^m w_i(x) d^2(y, y_i), \quad \sum_{i=1}^m w_i(x) = 1, \quad x \in \mathbb{R}^q. \quad (1)$$

Here \mathcal{M}_{ex} is the subset of the manifold on which we establish existence, and some weights $w_i(x)$ may be negative. Thus, the objective is an affine, rather than a convex combination of squared distances. This

***Funding:** This work was funded by the National Science Foundation, Grant #2443064.

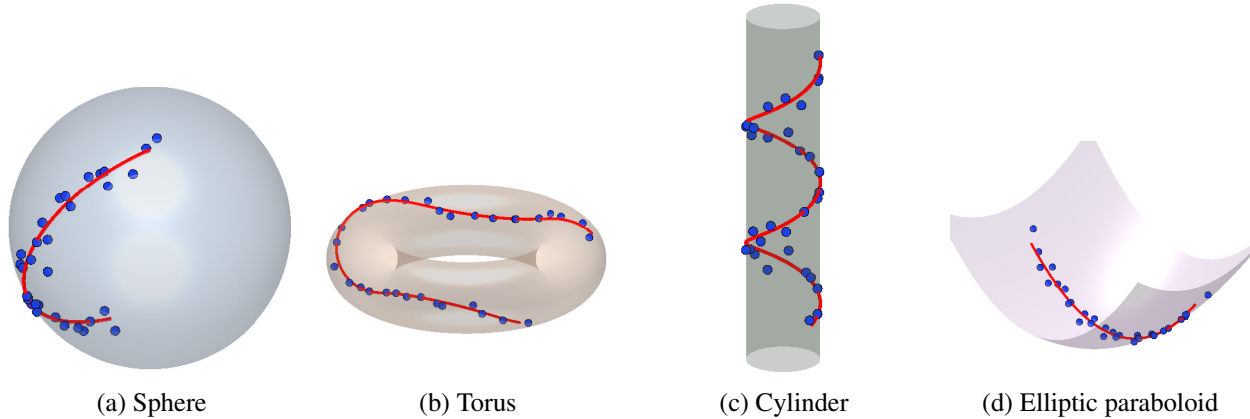


Figure 1: Illustration of Fréchet regression on four manifolds: the sphere, torus, cylinder, and elliptic paraboloid. In each panel, the surface (i.e., the manifold) is shown along with a geodesic regressor curve and noisy observations constrained to it.

signed structure enables extrapolation in predictor space and distinguishes Fréchet regression from ordinary barycenter estimation, but it also changes the optimization problem: minimizers may fail to exist or be unique, and standard barycenter convexity arguments no longer apply.

In Euclidean spaces, signed weighted barycenters have a natural difference-of-convex (DC) structure, linking them to DC programming and DCA literature [8, 10, 11, 15, 26, 29, 31]. On Hadamard manifolds, global geodesic convexity of squared distances enabled the authors in [5] to develop a Riemannian DCA with iterate convergence to critical points. These results, however, do not cover the positively or nonnegatively curved settings common in Fréchet regression. Figure 1 illustrates representative manifolds where responses follow a geodesic trajectory with noisy observations constrained to the manifold.

This obstruction is not pathological: it already occurs on spheres, where squared distances are smooth only away from the cut locus and are not globally geodesically convex; related center-of-mass and gradient-descent issues on manifolds of constant nonnegative curvature were studied in [1]. Similar difficulties arise on other nonnegatively curved manifolds, such as $SO(3)$ and real projective spaces [33]. They also appear in optimal transport: the Bures–Wasserstein manifold of nondegenerate Gaussian covariances has nonnegative sectional curvature [24], yet squared-distance averaging objectives on it are geodesically nonconvex [2]. Thus, nonnegative curvature naturally yields regression and barycenter objectives that are smooth on a suitable normal neighborhoods but lose geodesic convexity beyond a curvature-dependent scale.

This paper develops an optimization framework for signed Fréchet regression on complete Riemannian manifolds with controlled sectional curvature. Instead of optimizing over the full manifold, we work on a strongly convex normal ball \mathcal{M} containing the response support. On this safe set, logarithm maps are single-valued, squared distances are smooth, Hessian comparison gives local second-order bounds, and Jacobi-field estimates control the linearization of the concave part. We then decompose the signed objective as $f(y, x) = g(y) - h(y)$ (dependency on x is implicit), where g and h collect the positive- and negative-weight terms, and develop FRIDA, a Riemannian proximal DC method adapted to this local geometry.

Our contributions are fourfold. First, we prove the existence and interiority of stationary points for the signed Fréchet regression objective on the safe set. We give explicit conditions ensuring that the total negative weight is small enough for the objective to attain a minimum on \mathcal{M} , with every minimizer lying in $\text{int}(\mathcal{M})$ and hence stationary. We also translate these conditions into guarantees in predictor space, including finite-sample ellipsoidal sufficient conditions.

Second, we derive curvature-dependent estimates for the proposed proximal DC method under two-sided sectional-curvature bounds. The curvature upper bound controls the lower bounds on the Hessian for squared distances and hence the convexity radius, while the curvature lower bound controls the Jacobi-field

growth and the logarithm-Hessian smoothness constants. Together, these estimates yield computable lower bounds that ensure strong geodesic convexity of the proximal DC subproblems on a subset of the manifold.

Third, we propose exact and inexact versions of FRIDA using these estimates. The proximal DC subproblems are solved directly on the manifold, preserving feasibility by construction. We prove objective descent, boundedness of the iterates in the safe set, and stationarity of every accumulation point for the original signed Fréchet regression objective. We also derive explicit $O((N + 1)^{-1/2})$ sublinear complexity bounds for the smallest successive-step distance among the first $N + 1$ iterations.

Fourth, under an additional real-analyticity assumption on the manifold, we strengthen the convergence analysis via the Kurdyka–Łojasiewicz framework. In that case, the whole sequence converges to a single stationary point, and the local rate is determined by the KL exponent: finite termination when the exponent is zero, linear convergence for exponents in $(0, 1/2]$, and sublinear convergence otherwise.

The paper contributes to the intersection of Fréchet regression and Riemannian optimization. It provides an algorithmic foundation for evaluating global Fréchet regression with signed weights on curved response spaces, and develops FRIDA as a proximal DC framework for signed barycenter problems outside the Hadamard setting, where explicitly local geometric control is required.

The rest of the paper is organized as follows. Section 2 presents preliminary background and notation. Section 3 formulates the signed Fréchet regression problem and introduces the safe-set geometry. Section 4 establishes existence and interiority of minimizers. Section 5 shows the convergence analysis for the main convergence guarantees of exact and inexact FRIDA. Improved KL-based rates are shown in Section 6. Numerical analysis is shown in Section 7.

2 Background and notation

We work on a complete Riemannian manifold (Ω, d) with geodesic distance d . For $x \in \Omega$, $T_x\Omega$ denotes the tangent space, equipped with inner product $\langle \cdot, \cdot \rangle_x$ and norm $\|\xi\|_x = \sqrt{\langle \xi, \xi \rangle_x}$. In common normal neighborhoods, we use the exponential map \exp_x , its inverse \log_x , and parallel transport $P_{x \rightarrow y}$.

Definition 2.1 (Eq.(1.3)–(1.6) in [28]). Let R denote the Riemann curvature tensor on Ω , with convention $R(X, Y)Z = \nabla_X \nabla_Y Z - \nabla_Y \nabla_X Z - \nabla_{[X, Y]}Z$, and let ∇R denote its covariant derivative.

For a C^1 function $f : \Omega \rightarrow \mathbb{R}$, the Riemannian gradient $\text{grad } f(x) \in T_x\Omega$ is defined by

$$Df(x)[\xi] = \langle \text{grad } f(x), \xi \rangle_x,$$

for all $\xi \in T_x\Omega$. Whenever z and y lie in a common normal neighborhood, $\text{grad}_y(1/2)d^2(z, y) = -\log_y(z)$.

Definition 2.2. Let $\mathcal{X} \subset \Omega$ be geodesically convex and let $f : \mathcal{X} \rightarrow \mathbb{R}$ be C^1 . We say that f is μ -strongly geodesically convex on \mathcal{X} if

$$f(y) \geq f(x) + \langle \text{grad } f(x), \log_x(y) \rangle_x + \frac{\mu}{2}d^2(x, y), \quad \forall x, y \in \mathcal{X}.$$

We say that f is L -smooth on \mathcal{X} if $\|\text{grad } f(y) - P_{x \rightarrow y} \text{grad } f(x)\|_y \leq L d(x, y)$, $\forall x, y \in \mathcal{X}$.

Definition 2.3. Let $\mathcal{X} \subset \Omega$ be geodesically convex with $\text{diam}(\mathcal{X}) \leq D$, and assume $-\Lambda_- \leq \text{sec}_\Omega \leq \Lambda_+$ on \mathcal{X} , where $\Lambda_-, \Lambda_+ \geq 0$. Define $\delta_D \triangleq \delta_+(D)$, $\zeta_D \triangleq \zeta_-(D)$

$$\delta_+(t) \triangleq \begin{cases} t\sqrt{\Lambda_+} \cot(t\sqrt{\Lambda_+}), & \Lambda_+ > 0, \\ 1, & \Lambda_+ = 0, \end{cases} \quad \zeta_-(t) \triangleq \begin{cases} t\sqrt{\Lambda_-} \coth(t\sqrt{\Lambda_-}), & \Lambda_- > 0, \\ 1, & \Lambda_- = 0. \end{cases}$$

Also, define the logarithm-Hessian factors as

$$\alpha_+(t) \triangleq \frac{t\sqrt{\Lambda_+}}{\sin(t\sqrt{\Lambda_+})}, \quad b_-(t) \triangleq \frac{\sinh(t\sqrt{\Lambda_-})}{t\sqrt{\Lambda_-}}, \quad c_-(t) \triangleq \cosh(t\sqrt{\Lambda_-}),$$

with limiting value 1 when $\Lambda_{\pm} = 0$; here δ_+, ζ_- are the squared-distance Hessian-comparison constants.

Lemma 2.4 (Lemma 23 in [20]). *Let $\mathcal{X} \subset \Omega$ be geodesically convex with $\text{diam}(\mathcal{X}) \leq D$, and assume $-\Lambda_- \leq \sec\Omega \leq \Lambda_+$ on \mathcal{X} . If $\Lambda_+ > 0$, assume also $D < \pi/(2\sqrt{\Lambda_+})$. Then, for all $z, y \in \mathcal{X}$ and all $v \in T_y\Omega$,*

$$\delta_D \|v\|_y^2 \leq \text{Hess}_y \left(\frac{1}{2} d^2(z, y) \right) [v, v] \leq \zeta_D \|v\|_y^2.$$

Consequently, $y \mapsto \frac{1}{2} d^2(z, y)$ is δ_D -strongly convex and ζ_D -smooth on \mathcal{X} .

Definition 2.5. Let $\gamma : [0, \ell] \rightarrow \Omega$ be a geodesic. A vector field J along γ is a Jacobi field if

$$D_t^2 J + R(J, \dot{\gamma})\dot{\gamma} = 0,$$

where D_t denotes the covariant derivative along γ . If $\gamma(t) = \exp_p(tu)$ and $w \in T_p\Omega$, then the Jacobi field satisfying $J(0) = 0$ and $D_t J(0) = w$ is given by $J(t) = d(\exp_p)_{tu}(tw)$ [6, Chapter 5, Proposition 2.7].

Definition 2.6 (Ch. 1 in [16]). A Riemannian manifold is called real analytic if it admits an atlas with real-analytic transition maps.

Definition 2.7. Let Ω be a Riemannian manifold and let $f : \Omega \rightarrow \mathbb{R}$ be C^1 . We say that f satisfies the Riemannian Kurdyka–Łojasiewicz property at $\bar{x} \in \Omega$ if there exist a neighborhood U of \bar{x} , $\delta > 0$, and a concave function $\varphi : [0, \delta) \rightarrow [0, \infty)$ such that $\varphi(0) = 0$, $\varphi \in C^1(0, \delta)$, $\varphi'(s) > 0$ on $(0, \delta)$, and $\varphi'(f(x) - f(\bar{x})) \|\text{grad } f(x)\|_x \geq 1$ for all $x \in U$ satisfying $f(\bar{x}) < f(x) < f(\bar{x}) + \delta$.

Proposition 2.8 (Theorem 3.5 in [23] and Section 9 in [14]). *Let Ω be a real-analytic Riemannian manifold and let $f : \Omega \rightarrow \mathbb{R}$ be real analytic. Then f is locally Lipschitz and subanalytic; in particular, it is a locally Lipschitz \mathcal{C} -function. Hence f satisfies the Riemannian Kurdyka–Łojasiewicz property at every point of Ω .*

3 Problem Formulation

Let (Ω, d) be an n -dimensional complete Riemannian manifold with bounded sectional curvature, and consider a random pair $(X, Y) \sim \mathcal{P}$, where $X \in \mathbb{R}^q$ and $Y \in \Omega$ and \mathcal{P} is a joint distribution on $\mathbb{R}^q \times \Omega$. Additionally, assume the marginal distributions $X \sim \mathcal{P}_X$ and $Y \sim \mathcal{P}_Y$ exist. Moreover, assume $\mu = \mathbb{E}[X]$ and $\Sigma = \text{Var}(X)$ exist with $\Sigma \succ 0$. The Fréchet regression function [22] of Y given $X = x$, also known as the conditional barycenter of Y given $X = x$, is defined as

$$m(x) = \arg \min_{y \in \Omega} M(x, y) \triangleq \mathbb{E}[d^2(Y, y) \mid X = x]. \quad (2)$$

Classically (2) is solved by approximating it into a system of unconditional expectations [4, 9, 18]. Following the global Fréchet regression construction of [22], one can define the (unconstrained) global Fréchet regression function by

$$m_{\oplus}(x) \triangleq \arg \min_{y \in \Omega} M_{\oplus}(y, x), \quad M_{\oplus}(y, x) \triangleq \mathbb{E} \left[s(X, x) d^2(Y, y) \right], \quad (3)$$

where $s(z, x) = 1 + (z - \mu)^\top \Sigma^{-1}(x - \mu)$, and $\mathbb{E}[s(X, x)] = 1$. Moreover, for every fixed $x \in \mathbb{R}^q$, $\mathbb{E}|s(X, x)| < \infty$. In Euclidean spaces, Eq. (3) reproduces ordinary linear regression; on a general metric space, it should be viewed as a model-based global approximation to the conditional Fréchet mean.

In the sequel, we study the constrained problem

$$m_{\oplus}(x) \triangleq \arg \min_{y \in \mathcal{M}_{\text{ex}}} M_{\oplus}(y, x), \quad (4)$$

where $\mathcal{M}_{\text{ex}} \subset \Omega$ is a safe set where solutions are guaranteed to exist even in the presence of negative weights.

Similarly, if instead of the joint distribution \mathcal{P} , one has access to independent realizations of (x_i, y_i) for $i = 1, \dots, m$, with positive definite sample covariance, the estimator of the linear Fréchet regression function is defined as

$$\begin{aligned} \hat{m}_{\oplus}(x) &= \arg \min_{y \in \mathcal{M}_{\text{ex}}} \frac{1}{m} \sum_{i=1}^m s_{i,m}(x) d^2(y_i, y) \text{ with } \frac{1}{m} \sum_{i=1}^m s_{i,m}(x) = 1, \forall x \in \mathbb{R}^q, \\ s_{i,m}(x) &= 1 + (x_i - \hat{\mu})^\top \hat{\Sigma}^{-1}(x - \hat{\mu}), \quad \hat{\mu} = \frac{1}{m} \sum_{i=1}^m x_i, \quad \hat{\Sigma} = \frac{1}{m} \sum_{i=1}^m (x_i - \hat{\mu})(x_i - \hat{\mu})^\top \end{aligned}$$

The definition of the estimator $\hat{m}_{\oplus}(x)$ provides the function class of problems we will focus on in this paper. Specifically, for a given set of pairs $\{(x_i, y_i)\}_{i=1}^m$, where $x_i \in \mathbb{R}^q$ and $y_i \in \Omega$, we will focus on solving optimization problems of the form Eq. (1) where $w_i(x) = m^{-1}s_{i,m}(x)$ are possibly negative weights determined by the query point x and the observed covariates $\{x_i\}_{i=1}^m$. For the sake of simplicity in the subsequent analysis, we introduce the following notation for Problem (1), separating the summands into those with positive and negative weights.

$$\begin{aligned} \min_{y \in \mathcal{M}_{\text{ex}}} f(y, x) &\triangleq g(y) - h(y), \text{ where} \\ g(y) &= \sum_{w_i(x) \geq 0} w_i(x) d^2(y, y_i), \text{ and } h(y) = - \sum_{w_j(x) < 0} w_j(x) d^2(y, y_j). \end{aligned} \quad (5)$$

Note that implicit dependencies on x are omitted but should be clear from context. Moreover, for a given $x \in \mathbb{R}^q$, we define

$$w_+(x) = \sum_{w_i(x) \geq 0} w_i(x), \text{ and } w_-(x) = - \sum_{w_j(x) < 0} w_j(x).$$

Remark 3.1 (Global and local FRIDA). The weights $w_i(x) = m^{-1}s_{i,m}(x)$ defined above are the global affine weights of Fréchet regression. When Algorithm 1 is applied with these weights, we call the resulting method *global FRIDA*.

The same framework also covers local Fréchet regression by replacing the global weights with the local-linear weights in [22]. For $j = 0, 1, 2$,

$$w_{i,m}^{\text{loc}}(x) = \frac{1}{m} K_h(x_i - x) \frac{\mu_2(x) - \mu_1(x)(x_i - x)}{\mu_0(x)\mu_2(x) - \mu_1(x)^2}, \quad \mu_j(x) = \frac{1}{m} \sum_{i=1}^m K_h(x_i - x)(x_i - x)^j,$$

$K_h(u) = h^{-1}K(u/h)$ for a bandwidth $h > 0$. With standard kernels such as Gaussian, Epanechnikov, or quartic [7], Algorithm 1 with these weights is called *local FRIDA*.

Thus, global and local FRIDA differ only in the weights: after recomputing $w_+(x)$ and $w_-(x)$, the objective, DC splitting, and algorithm are unchanged. The admissible region may change, but FRIDA remains agnostic to the weight construction.

Remark 3.2. Problem (1) is not a barycenter computation based on a convex combination of squared distances; it is an affine combination, since some weights may be negative. In fact, it is common to have negative weights. For example, if the x_i sampled from X are $x_1 = 0, x_2 = 2, x_3 = 4$ and set $x = 1/2$, then the corresponding weights are: $w_1 = 17/24, w_2 = 1/3, w_3 = -1/24$. Generally, $w_i < 0$ if and only if $(x_i - \hat{\mu})^\top \hat{\Sigma}^{-1}(x - \hat{\mu}) < -1$. A simple sufficient condition for nonnegativity of all weights follows from Cauchy–Schwarz. Define $D \triangleq \max_{1 \leq i \leq m} \|\hat{\Sigma}^{-1/2}(x_i - \hat{\mu})\|_2$. Then $\|\hat{\Sigma}^{-1/2}(x - \hat{\mu})\|_2 \leq 1/D$ and $w_i(x) \geq 0, \forall i$. Depending on the geometry of the observed covariates, D can be large, in which case the sufficient nonnegativity region becomes small and negative weights may occur even for moderate values of $\|x\|_2$. Formally, the following lemma specifies the range of x values that yield negative weights for arbitrary data points in real space.

Lemma 3.3. *Let $x_1, \dots, x_m \in \mathbb{R}^q$ and without loss of generality, let $\hat{\mu} = 0, \hat{\Sigma} = I$. Then,*

$$w_i(x) \geq 0, \forall x \in \mathbb{X} \subseteq \mathbb{R}^q,$$

where $\mathbb{X} = \bigcap_{i=1}^m \{x \in \mathbb{R}^q : x_i^\top x \geq -1\}$.

Proof. In the whitened coordinates $\hat{\mu} = 0$ and $\hat{\Sigma} = I$, one has $w_i(x) = (1/m)(1 + x_i^\top x)$. Hence $w_i(x) \geq 0$ if and only if $x_i^\top x \geq -1$. Imposing this for all $i = 1, \dots, m$ yields the stated intersection of half-spaces. \square

The convergence analysis has three steps. We first identify a compact, well-posed region for the affine weighted objective. Second, we construct a proximal DC model that is strongly geodesically convex on smaller local balls. Third, we combine the resulting descent estimate with compactness to prove stationarity of accumulation points.

4 Existence of Solutions, FRIDA and Main Results

4.1 Existence of a Minimizer on a Safe Set

In this section, we isolate a compact geodesic ball containing all responses and show that the affine weighted objective attains a minimum there. A boundary-gradient condition then rules out boundary minimizers, so every minimizer is interior and therefore stationary. Strong convexity will only be needed later, on smaller local balls used in the proximal subproblems. We then specialize this criterion to finite-sample and ellipsoidal covariate regions.

Assumption 1. The Riemannian manifold (Ω, d) is complete and its sectional curvatures satisfy:

$$-\Lambda_- \leq \sec_\Omega \leq \Lambda_+ < \infty, \quad \Lambda_-, \Lambda_+ \geq 0.$$

Assumption 2. There exists $c \in \Omega$ and $r > 0$ such that $\mathbb{P}(Y \in B_r(c)) = 1$.

Assumption 3. There exists $\rho_{\text{ex}} > 0$ such that $r < \rho_{\text{ex}} < \min\{\iota_{r,c}, \pi/\sqrt{\Lambda_+}\} - r$.

Assumption 4. There exists $\rho > 0$ such that $r < \rho < \min\{(1/2)\iota_{\rho_{\text{ex}},c}, \pi/(2\sqrt{\Lambda_+})\}$.

Assumptions 2–3 define the existence-safe ball $\mathcal{M}_{\text{ex}} \triangleq \overline{B_{\rho_{\text{ex}}}(c)}$, which contains $\mathcal{M}_r \triangleq \overline{B_r(c)}$ with a positive injectivity margin. Indeed, for any $z \in \mathcal{M}_r$ and $y \in \mathcal{M}_{\text{ex}}$, $d(z, y) \leq r + \rho_{\text{ex}} < \iota_{r,c} \leq \text{inj}_\Omega(z)$. Thus, $d^2(z, y)$, and $M_{\oplus}(\cdot, x)$ are smooth on \mathcal{M}_{ex} with respect to y . Assumption 4 introduces the smaller algorithmic ball $\mathcal{M}_\rho \triangleq \overline{B_\rho(c)}$. Since $2\rho < \iota_{\rho,c}$ and $\rho < \pi/(2\sqrt{\Lambda_+})$, \mathcal{M}_ρ is a strongly convex normal ball [30, Lemma 3.2.1]; in particular, $\log_x(y)$ is well defined for all $x, y \in \mathcal{M}_\rho$, and every two points of \mathcal{M}_ρ are joined by a unique minimizing geodesic in \mathcal{M}_ρ . Finally, Assumption 1 gives the two-sided curvature

control used below: Λ_+ controls the lower Hessian-comparison constants, while Λ_- controls the upper smoothness constants. Set

$$\delta_{\text{ex}} \triangleq \delta_+(r + \rho_{\text{ex}}), \quad \zeta_{\text{ex}} \triangleq \zeta_-(r + \rho_{\text{ex}}), \quad L_R \triangleq \sup_{q \in \mathcal{M}_{\text{ex}}} \|(\nabla R)_q\|, \quad \Lambda_0 \triangleq \max\{\Lambda_+, \Lambda_-\}.$$

Since \mathcal{M}_{ex} is compact and $R, \nabla R$ are smooth, $L_R < \infty$, and $\|R_q\| \leq c_n \Lambda_0$ on \mathcal{M}_{ex} for some $c_n > 0$ depending only on n and the tensor norm [27, Proposition 1.1].

Theorem 4.1. *Let Assumptions 1–3 hold, for every fixed $x \in \mathbb{R}^q$ such that $\mathbb{E}|s(X, x)| < \infty$, the objective $M_{\oplus}(\cdot, x)$ attains a minimum on \mathcal{M}_{ex} . If, in addition,*

$$\mathbb{E}[(s(X, x))_-] < (\rho_{\text{ex}} - r)/(2r), \tag{6}$$

then every minimizer $y^* \in \text{int}(\mathcal{M}_{\text{ex}})$ and is stationary, i.e., $\text{grad}_y M_{\oplus}(y^*, x) = 0$.

Proof. We first show that $M_{\oplus}(\cdot, x)$ is well defined and attains a minimum on \mathcal{M}_{ex} . By Assumption 2, $Y \in B_r(c)$ almost surely, so for every $y \in \mathcal{M}_{\text{ex}}$,

$$d(Y, y) \leq d(Y, c) + d(c, y) \leq r + \rho_{\text{ex}} \quad \text{a.s.}$$

Hence $|s(X, x)| d^2(Y, y) \leq (r + \rho_{\text{ex}})^2 |s(X, x)|$, and the right-hand side is integrable. Therefore $M_{\oplus}(y, x)$ is finite for every $y \in \mathcal{M}_{\text{ex}}$. For every $z \in \mathcal{M}_r$, the map $d^2(z, y)$ is smooth on \mathcal{M}_{ex} , and

$$\sup_{z \in \mathcal{M}_r, y \in \mathcal{M}_{\text{ex}}} \|\text{grad}_y d^2(z, y)\|_y \leq 2(r + \rho_{\text{ex}}) < \infty.$$

Thus, dominated convergence allows differentiation under the expectation, so $M_{\oplus}(\cdot, x) \in C^1(\mathcal{M}_{\text{ex}})$. Since (Ω, d) is complete, Hopf–Rinow implies that the closed bounded ball \mathcal{M}_{ex} is compact. Hence $M_{\oplus}(\cdot, x)$ attains a minimum on \mathcal{M}_{ex} .

Now let $y \in \partial \mathcal{M}_{\text{ex}}$, and let $\nu_y \triangleq \text{grad } d(c, \cdot)|_y$ be the outward unit normal. By [30, Lem. 3.4.8], for every $z \in \mathcal{M}_r$, $\langle -\log_y(z), \nu_y \rangle_y \geq \rho_{\text{ex}} - r$. Also,

$$\|-\log_y(z)\|_y = d(y, z) \leq \rho_{\text{ex}} + r.$$

$$\text{Therefore } \langle \text{grad}_y M_{\oplus}(y, x), \nu_y \rangle_y \geq 2(\rho_{\text{ex}} - r)\mathbb{E}[(s(X, x))_+] - 2(\rho_{\text{ex}} + r)\mathbb{E}[(s(X, x))_-].$$

Since $\mathbb{E}[(s(X, x))_+] - \mathbb{E}[(s(X, x))_-] = 1$, condition (6) implies

$$(\rho_{\text{ex}} - r)\mathbb{E}[(s(X, x))_+] - (\rho_{\text{ex}} + r)\mathbb{E}[(s(X, x))_-] = \rho_{\text{ex}} - r - 2r \mathbb{E}[(s(X, x))_-] > 0.$$

Thus, the outward directional derivative is strictly positive on $\partial \mathcal{M}_{\text{ex}}$, so no minimizer can lie on the boundary. Hence, every minimizer y^* lies in $\text{int}(\mathcal{M}_{\text{ex}})$, and the first-order necessary condition gives

$$\text{grad}_y M_{\oplus}(y^*, x) = 0.$$

□

Theorem 4.1 shows that if the total negative weight is not too large, then minimizers exist and cannot occur on the boundary of the safe ball.

Corollary 4.2. *Let Assumptions 1, 2, and 3 hold. If*

$$x \in \mathcal{X}_{\text{ex}}, \quad \mathcal{X}_{\text{ex}} \triangleq \left\{ x \in \mathbb{R}^q : (x - \mu)^\top \Sigma^{-1} (x - \mu) < (\rho_{\text{ex}}/r)^2 - 1 \right\},$$

then $M_{\oplus}(\cdot, x)$ attains a minimum in $\text{int}(\mathcal{M}_{\text{ex}})$ and is stationary.

Corollary 4.3. Let $\{(x_i, y_i)\}_{i=1}^m$ be m i.i.d. realizations of $(X, Y) \sim \mathcal{P}$, and let Assumptions 1, 2, and 3 hold. For every fixed $x \in \mathbb{R}^q$, if $w_-(x) < (\rho_{\text{ex}} - r)/(2r)$, then $f(\cdot, x)$ in (5) has an interior minimizer in \mathcal{M}_{ex} ; every minimizer is stationary. Moreover, the same result follows if alternatively

$$x \in \widehat{\mathcal{X}}_{\text{ex}}, \quad \widehat{\mathcal{X}}_{\text{ex}} \triangleq \left\{ x \in \mathbb{R}^q : (x - \hat{\mu})^\top \hat{\Sigma}^{-1} (x - \hat{\mu}) < (\rho_{\text{ex}}/r)^2 - 1 \right\}$$

Corollary 4.2 gives a convenient sufficient condition directly in covariate space: an explicit ellipsoidal region where existence and interior stationarity are guaranteed on \mathcal{M}_{ex} . Corollary 4.3 is the exact finite-sample analog of Theorem 4.1: the population negative-weight condition is replaced by its empirical counterpart, and the conclusion holds on \mathcal{M}_{ex} . It also provides a directly computable safe extrapolation region from the observed covariates for the larger existence-safe ball \mathcal{M}_{ex} .

The results in this section identify concrete geometric regions in covariate space where minimizers are guaranteed to exist and, moreover, are forced to lie strictly inside the existence-safe ball \mathcal{M}_{ex} , we thus define $f_* \triangleq \min_{y \in \mathcal{M}_{\text{ex}}} f(y, x)$.

4.2 FRIDA: Riemannian Iterative DC Algorithm and Main Results

The previous subsection guarantees that the objective is well defined on the existence-safe set \mathcal{M}_{ex} . We now introduce the method FRIDA: Fréchet Regression via Riemannian Iterative DC Algorithm, which builds upon a proximal DC step on an adaptive local ball $\mathcal{M}_k \subset \mathcal{M}_{\text{ex}}$, chosen so that the linearization of the concave part remains controlled and the proximal model is strongly geodesically convex.

Algorithm 1 FRIDA: Fréchet Regression via Riemannian Iterative DC Algorithm

Inputs: $y_0 \in \text{int}(\mathcal{M}_{\text{ex}})$, $\zeta = 1/4$, $x \in \mathbb{R}^q$, $\rho > 0$, curvature constants $\Lambda_\pm, L_R, c_n, \epsilon_k > 0$ with $\sum_{k=0}^\infty \epsilon_k < \infty$, $\theta \in (0, 1)$, $\eta_0 > 0$, and $\delta_{\text{ex}} \triangleq \delta_+(r + \rho_{\text{ex}})$.

- 1: **for** $k = 0, 1, 2, \dots$ **do**
- 2: Choose $r_k = \min\{\theta \text{dist}(y_k, \partial\mathcal{M}_{\text{ex}}), \rho\}$, and $\mathcal{M}_k = \overline{B_{r_k}(y_k)}$.
- 3: Set $\delta_k \triangleq \delta_+(r_k)$ and $L_{\log}^\pm(r_k) \triangleq \alpha_+(r_k)^3 \left[\frac{1}{6} L_R r_k^2 b_-(r_k)^3 + \frac{5}{6} c_n \Lambda_0 r_k b_-(r_k)^2 c_-(r_k) \right]$.
- 4: Set $\tau_k = \max \left\{ \frac{L_{\log}^\pm(r_k) \|\text{grad } h(y_k)\| - 2w_+(x)\delta_{\text{ex}}}{\delta_+(r_k)} + \frac{2\|\text{grad } f(y_k)\|}{\delta_+(r_k)r_k} + \eta_0, 1 - 2w_-(x)\delta_{\text{ex}}, 1 \right\}$.
- 5: Compute y_{k+1} according to one of the following cases:
- 6: **Exact Method:**
- 7: $y_{k+1} = \arg \min_{y \in \mathcal{M}_k} \Phi_k(y) \triangleq \left\{ g(y) - \langle \text{grad } h(y_k), \log_{y_k}(y) \rangle + \frac{\tau_k}{2} d^2(y_k, y) \right\}$
- 8: **Inexact Method:**
- 9: Find $\hat{y} \in \mathcal{M}_k$ s.t. $\|\text{grad } \Phi_k(\hat{y})\| \leq \min(\epsilon_k, \zeta d(y_k, \hat{y}))$, and $\Phi_k(\hat{y}) \leq \Phi_k(y_k)$
- 10: $y_{k+1} = \hat{y}$.
- 11: **end for**

Theorem 4.4. Let $\{(x_i, y_i)\}_{i=1}^m$ be m i.i.d. realizations of $(X, Y) \sim \mathcal{P}$, and let Assumptions 1–4 hold. Fix $x \in \mathbb{R}^q$ such that $w_-(x) < (\rho_{\text{ex}} - r)/(2r)$. Assume that $y_0 \in \text{int}(\mathcal{M}_{\text{ex}})$ and $f(y_0, x) < \min_{y \in \partial\mathcal{M}_{\text{ex}}} f(y, x)$. Let $\{y_k\}$ be the sequence generated by Algorithm 1. Then:

1. The sequence $\{y_k\} \subset \mathcal{M}_{\text{ex}}$ has at least one accumulation point $\bar{y} \in \mathcal{M}_{\text{ex}}$
2. Every accumulation point \bar{y} is stationary for $f(\cdot, x)$, i.e. $\text{grad } f(\bar{y}, x) = 0$.
3. For every $N \in \mathbb{N}$, the following estimates hold:

$$\min_{0 \leq k \leq N} d(y_k, y_{k+1}) \leq \sqrt{\frac{f(y_0, x) - f_*}{\kappa(N+1)}}, \quad \kappa = \begin{cases} 1/2, & \text{Exact Method,} \\ 1/4, & \text{Inexact Method} \end{cases} \quad (7)$$

The strict sublevel assumption on y_0 ensures that all iterates remain in a compact subset of $\text{int}(\mathcal{M})$, which in turn provides a uniform positive distance from the boundary and allows the proximal parameters τ_k to be chosen uniformly bounded.

5 Convergence Analysis

The proof uses three ingredients: (i) Hessian control of the linearized concave part, (ii) strong convexity of proximal subproblems, and (iii) a decrease estimate yielding vanishing steps and stationarity of accumulation points.

5.1 Subproblem Strong Convexity and Closed Iterations

Next, we provide the local geometry needed by the proximal model. The first controls the Hessian of the linearized concave term $y \mapsto \langle \xi, \log_p(y) \rangle$, while the second gives lower and upper Hessian bounds for the positive and negative weighted squared-distance terms.

Lemma 5.1. *Let Assumptions 1, 3, and 4 hold. Fix $p \in \text{int}(\mathcal{M}_{\text{ex}})$, $\xi \in T_p\Omega$, and let*

$$0 < r_p < \min\{\text{dist}(p, \partial\mathcal{M}_{\text{ex}}), \rho\}.$$

For $y \in \overline{B_{r_p}(p)} \setminus \{p\}$, define

$$\psi(y) \triangleq \langle \xi, \log_p(y) \rangle,$$

$\beta \triangleq d(p, y)$. Then, for every $v \in T_y\Omega$, set $\Lambda_0 \triangleq \max\{\Lambda_+, \Lambda_-\}$ and

$$|\text{Hess}_y \psi(v, v)| \leq L_{\log}^{\pm}(\beta) \|\xi\| \|v\|^2, \\ \text{where } L_{\log}^{\pm}(\beta) \triangleq \alpha_+(\beta)^3 \left[\frac{1}{6} L_R \beta^2 b_-(\beta)^3 + \frac{5}{6} c_n \Lambda_0 \beta b_-(\beta)^2 c_-(\beta) \right].$$

Proof. Let $u \triangleq \log_p(y)$, so $\beta = \|u\| = d(p, y) \leq r_p \leq \rho$. By Lemma 5.3, $\overline{B_{r_p}(p)}$ is a strongly convex normal ball. Hence $A_u \triangleq (d \exp_p)_u$ is invertible, the geodesic $\eta(\tau) \triangleq \exp_p(\tau u)$, $\tau \in [0, 1]$, is the unique minimizing geodesic from p to y , and $\eta([0, 1]) \subset \overline{B_{r_p}(p)} \subset \mathcal{M}_{\text{ex}}$. Thus along η we use $\|R\| \leq c_n \Lambda_0$ and $\|\nabla R\| \leq L_R$. Let $\gamma : (-\varepsilon, \varepsilon) \rightarrow \Omega$ be the geodesic with $\gamma(0) = y$ and $\dot{\gamma}(0) = v$, and define $Y(t) \triangleq \log_p(\gamma(t))$. Since $\exp_p(Y(t)) = \gamma(t)$, differentiation gives $A_{Y(t)} Y'(t) = \dot{\gamma}(t)$. Differentiating covariantly in t and evaluating at $t = 0$ yields

$$(\nabla_{Y'(0)} A)_u Y'(0) + A_u Y''(0) = 0,$$

because γ is geodesic. Since $\psi(\gamma(t)) = \langle \xi, Y(t) \rangle$,

$$\text{Hess}_y \psi(v, v) = \left. \frac{d^2}{dt^2} \right|_{t=0} \psi(\gamma(t)) = \langle \xi, Y''(0) \rangle,$$

$$|\text{Hess}_y \psi(v, v)| \leq \|\xi\| \|A_u^{-1}\| \|(\nabla_{Y'(0)} A)_u Y'(0)\|.$$

We first show $\|A_u^{-1}\| \leq \alpha_+(\beta)$. For $w \in T_p\Omega$, decompose $w = w^{\parallel} + w^{\perp}$, where $w^{\parallel} \in \mathbb{R}u$ and $w^{\perp} \perp u$. The radial part is preserved: $\|A_u(w^{\parallel})\| = \|w^{\parallel}\|$. For the orthogonal part, let $\hat{u} = u/\beta$, $\bar{\eta}(s) \triangleq \exp_p(s\hat{u})$,

$0 \leq s \leq \beta$, and $\tilde{J}(s) \triangleq (d \exp_p)_{s\tilde{u}}(s w^\perp / \beta)$. Then \tilde{J} is an orthogonal Jacobi field along the unit-speed geodesic $\tilde{\eta}$ with $\tilde{J}(0) = 0$, $D_s \tilde{J}(0) = w^\perp / \beta$, and $\tilde{J}(\beta) = A_u(w^\perp)$. By the metric comparison theorem [17, Thm. 11.10] with the upper sectional-curvature bound Λ_+ gives

$$\|A_u(w^\perp)\| = \|\tilde{J}(\beta)\| \geq (\sin(\sqrt{\Lambda_+}\beta) / (\sqrt{\Lambda_+}\beta)) \|w^\perp\| = \alpha_+(\beta)^{-1} \|w^\perp\|.$$

By Gauss' lemma [17, Thm. 6.9], $A_u(w^\parallel) \perp A_u(w^\perp)$, hence $\|A_u w\| \geq \alpha_+(\beta)^{-1} \|w\|$, so

$$\|A_u^{-1}\| \leq \alpha_+(\beta), \quad \|Y'(0)\| = \|A_u^{-1}v\| \leq \alpha_+(\beta)\|v\|.$$

Next, we estimate $(\nabla_\zeta A)_u w$. Fix $\zeta, w \in T_p \Omega$, set

$$s_\varepsilon \triangleq u + \varepsilon \zeta, \quad \eta_\varepsilon(\tau) \triangleq \exp_p(\tau s_\varepsilon), \quad \text{and} \quad J^\varepsilon(\tau) \triangleq (d \exp_p)_{\tau s_\varepsilon}(\tau w).$$

Let $\eta = \eta_0$, $U \triangleq \partial_\tau \eta_\varepsilon|_{\varepsilon=0} = \dot{\eta}$, $V \triangleq \partial_\varepsilon \eta_\varepsilon|_{\varepsilon=0}$, $J \triangleq J^0$, and $Z \triangleq d_\varepsilon J^\varepsilon|_{\varepsilon=0}$. Since $J^\varepsilon(1) = A_{u+\varepsilon\zeta} w$, we have $Z(1) = (\nabla_\zeta A)_u w$.

Also $Z(0) = 0$, $D_\tau Z(0) = 0$, and differentiating the Jacobi equation for J^ε gives

$$D_\tau^2 Z + R(Z, U)U = -F$$

where

$$\begin{aligned} F &= (\nabla_U R)(V, U)J + (\nabla_V R)(J, U)U + R(D_\tau V, U)J \\ &\quad + 2R(V, U)D_\tau J + R(J, D_\tau V)U + R(J, U)D_\tau V. \end{aligned}$$

We now replace the nonnegative-curvature Jacobi estimates by the corresponding hyperbolic comparison estimates. Let W be any Jacobi field along η with $W(0) = 0$ and $D_\tau W(0) = a$. Write the same field in the unit-speed parameter $s = \beta\tau$ as $\widehat{W}(s) \triangleq W(s/\beta)$. Then $\widehat{W}(0) = 0$ and $D_s \widehat{W}(0) = a/\beta$. By Rauch comparison [17, Thm. 11.9] under the lower sectional-curvature bound $\sec_\Omega \geq -\Lambda_-$, we have

$$\|\widehat{W}(s)\| \leq s b_-(s) \|a/\beta\|, \quad \|D_s \widehat{W}(s)\| \leq c_-(s) \|a/\beta\|.$$

Returning to $s = \beta\tau$, and using the monotonicity of b_- and c_- , gives

$$\|W(\tau)\| \leq \tau b_-(\beta\tau) \|a\| \leq \tau b_-(\beta) \|a\|,$$

$$\|D_\tau W(\tau)\| = \beta \|D_s \widehat{W}(\beta\tau)\| \leq c_-(\beta\tau) \|a\| \leq c_-(\beta) \|a\|.$$

Applying these estimates to J and V , and using $\|U\| = \beta$, we obtain

$$\|J(\tau)\| \leq \tau b_-(\beta) \|w\|, \quad \|D_\tau J(\tau)\| \leq c_-(\beta) \|w\|, \quad \|V(\tau)\| \leq \tau b_-(\beta) \|\xi\|, \quad \|D_\tau V(\tau)\| \leq c_-(\beta) \|\xi\|.$$

and therefore $\|F(\tau)\| \leq (2L_R \beta^2 \tau^2 b_-(\beta)^2 + 5c_n \Lambda_0 \beta \tau b_-(\beta) c_-(\beta)) \|\xi\| \|w\|$.

For $s \in [0, 1]$ and $a \in T_{\eta(s)} \Omega$, let G_s^a be the Jacobi field on $[s, 1]$ solving

$$D_\tau^2 G_s^a + R(G_s^a, U)U = 0, \quad G_s^a(s) = 0, \quad D_\tau G_s^a(s) = a.$$

By the previous estimate, $\|G_s^a(1)\| \leq (1-s)b_-(\beta(1-s))\|a\| \leq (1-s)b_-(\beta)\|a\|$. Define

$$\tilde{Z}(\tau) \triangleq - \int_0^\tau G_s^{F(s)}(\tau) ds.$$

A direct differentiation under the integral sign shows that \tilde{Z} satisfies the same inhomogeneous Jacobi equation and initial conditions as Z , hence $\tilde{Z} = Z$. Thus,

$$\|Z(1)\| \leq b_-(\beta) \int_0^1 (1-s) \|F(s)\| ds \leq \left(\frac{1}{6} L_R \beta^2 b_-(\beta) + \frac{5}{6} c_n \Lambda_0 \beta b_-(\beta)^2 c_-(\beta) \right) \|\zeta\| \|w\|.$$

Since $Z(1) = (\nabla_\zeta A)_u w$, we have proved

$$\|(\nabla_\zeta A)_u w\| \leq \left(\frac{1}{6} L_R \beta^2 b_-(\beta) + \frac{5}{6} c_n \Lambda_0 \beta b_-(\beta)^2 c_-(\beta) \right) \|\zeta\| \|w\|.$$

Finally choose $\zeta = w = Y'(0)$. Then combined with $\|Y'(0)\| \leq \alpha_+(\beta) \|v\|$,

$$\begin{aligned} \|Y''(0)\| &\leq \|A_u^{-1}\| \|(\nabla_{Y'(0)} A)_u Y'(0)\| \\ &\leq \alpha_+(\beta) \left(\frac{1}{6} L_R \beta^2 b_-(\beta) + \frac{5}{6} c_n \Lambda_0 \beta b_-(\beta)^2 c_-(\beta) \right) \|Y'(0)\|^2 \\ &\leq \alpha_+(\beta)^3 \left(\frac{1}{6} L_R \beta^2 b_-(\beta) + \frac{5}{6} c_n \Lambda_0 \beta b_-(\beta)^2 c_-(\beta) \right) \|v\|^2 \end{aligned}$$

Thus $|\text{Hess}_y \psi(v, v)| \leq L_{\log}^\pm(\beta) \|\xi\| \|v\|^2$ □

The next lemma provides a global lower bound on the Hessian of g and smoothness estimates for g and h . This lower bound need not be positive, so positivity in the proximal model will be recovered from the local proximal term on $\overline{B_{r_k}(y_k)}$.

Lemma 5.2. *Let Assumptions 1 and 2 hold. For every $z \in \mathcal{M}_r$, $y \in \mathcal{M}_{\text{ex}}$, and $v \in T_y \Omega$, yields $\delta_{\text{ex}} \|v\|^2 \leq \text{Hess}_y((1/2)d^2(z, y))(v, v) \leq \zeta_{\text{ex}} \|v\|^2$, and therefore*

$$2w_+(x) \delta_{\text{ex}} \|v\|^2 \leq \text{Hess}_y g(v, v) \leq 2w_+(x) \zeta_{\text{ex}} \|v\|^2,$$

$$2w_-(x) \delta_{\text{ex}} \|v\|^2 \leq \text{Hess}_y h(v, v) \leq 2w_-(x) \zeta_{\text{ex}} \|v\|^2.$$

Proof. If $y = z$, then $\text{Hess}_y(\frac{1}{2}d^2(z, \cdot))(v, v) = \|v\|^2$, so the claim is immediate. Assume henceforth that $y \neq z$. Define $\rho_z(y) \triangleq d(z, y)$. Then $\rho_z(y) \leq d(z, c) + d(c, y) \leq r + \rho_{\text{ex}}$. Moreover, $r + \rho_{\text{ex}} < \text{inj}_\Omega(z)$, so ρ_z is smooth at y . By Lemma 2.4

$$\delta_+(\rho_z(y)) \|v\|_y^2 \leq \text{Hess}_y \left(\frac{1}{2} d^2(z, y) \right) [v, v] \leq \zeta_-(\rho_z(y)) \|v\|_y^2.$$

Since δ_+ is decreasing, ζ_- is increasing, and $\rho_z(y) \leq r + \rho_{\text{ex}}$,

$$\delta_+(\rho_z(y)) \geq \delta_+(r + \rho_{\text{ex}}) = \delta_{\text{ex}}, \quad \zeta_-(\rho_z(y)) \leq \zeta_-(r + \rho_{\text{ex}}) = \zeta_{\text{ex}}.$$

Summing the inequalities termwise gives the bounds for g and h . □

Lemma 5.3. *Let Assumptions 1, 3, and 4 hold. Fix $p \in \text{int}(\mathcal{M}_{\text{ex}})$ and let*

$$0 < r_p < \min\{\text{dist}(p, \partial \mathcal{M}_{\text{ex}}), \rho\}.$$

Then $B_{r_p}(p)$ is a strongly convex normal ball. Moreover, $y \mapsto \frac{1}{2}d^2(p, y)$ is $\delta_+(r_p)$ -strongly geodesically convex on $\overline{B_{r_p}(p)}$.

Proof. Since $p \in \mathcal{M}_{\text{ex}}$, $\text{inj}_\Omega(p) \geq \nu_{\rho_{\text{ex}}, c}$, and $r_p < \text{dist}(p, \partial\mathcal{M}_{\text{ex}})$, we have $\overline{B_{r_p}(p)} \subset \mathcal{M}_{\text{ex}}$, and $B_{r_p}(p)$ is a strongly convex normal ball by [30, Lem. 3.2.1].

Now fix $y \in \overline{B_{r_p}(p)}$. If $y = p$, then $\text{Hess}_p((1/2)d^2(p, \cdot))(v, v) = \|v\|^2 \geq \delta_+(r_p)\|v\|^2$, since $\delta_+(r_p) \leq 1$. If $y \neq p$, define $\ell = d(p, y)$. Then $\ell \leq r_p < \pi/(2\sqrt{\Lambda_+})$, and the Hessian comparison theorem for the distance function [17, Thm. 11.7] gives

$$\text{Hess}_y((1/2)d^2(z, y))(v, v) \geq \delta_+(\ell)\|v\|^2.$$

Since δ_+ is decreasing and $\ell \leq r_p$, $\delta_+(\ell) \geq \delta_+(r_p)$, hence $\text{Hess}_y((1/2)d^2(p, y))(v, v) \geq \delta_+(r_p)\|v\|^2$.

Finally, let $\gamma : [0, 1] \rightarrow \overline{B_{r_p}(p)}$ be any minimizing geodesic. Because $B_{r_p}(p)$ is strongly convex, $\gamma([0, 1]) \subset B_{r_p}(p)$. Therefore

$$\frac{d^2}{dt^2}((1/2)d^2(p, \gamma(t))) = \text{Hess}_{\gamma(t)}((1/2)d^2(p, \cdot))(\dot{\gamma}(t), \dot{\gamma}(t)) \geq \delta_+(r_p)\|\dot{\gamma}(t)\|^2.$$

The standard one-dimensional characterization of strong convexity along geodesics now yields $\delta_+(r_p)$ -strong geodesic convexity on $\overline{B_{r_p}(p)}$. \square

The next proposition deduces that the chosen value of τ ensures that Φ_k is strongly convex by combining the Hessian bounds obtained above for each term.

Proposition 5.4. *Let Assumptions 1, 2, 3, and 4 hold. Fix $p \in \text{int}(\mathcal{M}_{\text{ex}})$, and let*

$$0 < r_p < \min\{\text{dist}(p, \partial\mathcal{M}_{\text{ex}}), \rho\},$$

and

$$\begin{aligned} \tau &> (L_{\log}^\pm(r_p)\|\text{grad } h(p)\| - 2w_+(x)\delta_{\text{ex}})/\delta_+(r_p), \\ L_{\log}^\pm(r_k) &\triangleq \alpha_+(r_k)^3 \left[\frac{1}{6}LRr_k^2b_-(r_k)^3 + \frac{5}{6}c_n\Lambda_0r_kb_-(r_k)^2c_-(r_k) \right], \quad 0 \leq t \leq \rho, \end{aligned}$$

then $\Phi_p(y)$ is $\mu(p, \tau)$ -strongly geodesically convex on $\overline{B_{r_p}(p)}$, where

$$\mu(p, \tau) \triangleq 2w_+(x)\delta_{\text{ex}} + \tau\delta_+(r_p) - L_{\log}^\pm(r_p)\|\text{grad } h(p)\| > 0.$$

Proof. Let $y \in \overline{B_{r_p}(p)}$ and $v \in T_y\Omega$. Then

$$\text{Hess}_y \Phi_p(v, v) = \text{Hess}_y g(v, v) - \text{Hess}_y(\langle \text{grad } h(p), \log_p(y) \rangle)(v, v) + \frac{\tau}{2} \text{Hess}_y d^2(p, y)(v, v).$$

Since $\overline{B_{r_p}(p)} \subset \mathcal{M}_{\text{ex}}$, Lemma 5.2 gives $\text{Hess}_y g(v, v) \geq 2w_+(x)\delta_{\text{ex}}\|v\|^2$.

Next, Lemma 5.1 applied with $\xi = \text{grad } h(p)$ yields

$$|\text{Hess}_y(\langle \text{grad } h(p), \log_p(y) \rangle)(v, v)| \leq L_{\log}^\pm(\beta)\|\text{grad } h(p)\|\|v\|^2, \quad \beta \triangleq d(p, y).$$

Because $\beta \leq r_p \leq \rho$ and $t \mapsto L_{\log}^\pm(t)$ is nondecreasing on $[0, \rho]$,

$$|\text{Hess}_y(\langle \text{grad } h(p), \log_p(y) \rangle)(v, v)| \leq L_{\log}^\pm(r_p)\|\text{grad } h(p)\|\|v\|^2.$$

Finally, Lemma 5.3 implies $\frac{\tau}{2} \text{Hess}_y d^2(p, y)(v, v) \geq \tau\delta_+(r_p)\|v\|^2$, and,

$$\text{Hess}_y \Phi_p(v, v) \geq \left(2w_+(x)\delta_{\text{ex}} + \tau\delta_+(r_p) - L_{\log}^\pm(r_p)\|\text{grad } h(p)\| \right) \|v\|^2 = \mu(p, \tau)\|v\|^2.$$

By the assumed lower bound on τ , $\mu(p, \tau) > 0$. Since $\overline{B_{r_p}(p)}$ is a strongly convex normal ball by Lemma 5.3, this lower Hessian bound implies that Φ_p is $\mu(p, \tau)$ -strongly geodesically convex on $\overline{B_{r_p}(p)}$. \square

While Proposition 5.4 guarantees strong convexity of Φ_p on $\overline{B_{r_p}(p)}$, the next lemma adds a further condition ensuring that its unique minimizer lies in $B_{r_p}(p) \subset \mathcal{M}_{\text{ex}}$.

Lemma 5.5. *Let Assumptions 1–4 hold. Fix $p \in \text{int}(\mathcal{M}_{\text{ex}})$, let $\theta \in (0, 1)$, and*

$$r_p = \min\left\{\theta \text{dist}(p, \partial\mathcal{M}_{\text{ex}}), \rho\right\}, \quad \tau > \frac{L_{\log}^{\pm}(r_p)\|\text{grad } h(p)\| - 2w_+(x)\delta_{\text{ex}}}{\delta_+(r_p)} + \frac{2\|\text{grad } f(p)\|}{\delta_+(r_p)r_p}.$$

Then Φ_p admits a unique minimizer on $B_{r_p}(p) \subset \mathcal{M}_{\text{ex}}$.

Proof. By Lemma 5.3, $\overline{B_{r_p}(p)}$ is a strongly convex normal ball. By Proposition 5.4, the above bound on τ implies that Φ_p is strongly geodesically convex on $\overline{B_{r_p}(p)}$. Since $\overline{B_{r_p}(p)}$ is compact, Φ_p attains a unique minimizer there.

It remains to show that the minimizer cannot lie on $\partial B_{r_p}(p)$. Let $z \in \partial B_{r_p}(p)$, and let $\gamma : [0, r_p] \rightarrow \overline{B_{r_p}(p)}$ be the unique unit-speed minimizing geodesic from p to z . Set $\varphi(t) \triangleq \Phi_p(\gamma(t))$. Strong geodesic convexity gives $\varphi''(t) \geq \mu(p, \tau) > 0$, on $t \in [0, r_p]$. Integrating we get, $\varphi'(r_p) \geq \varphi'(0) + \mu(p, \tau)r_p$. Since $\text{grad } \Phi_p(p) = \text{grad } f(p)$,

$$\varphi'(0) = \langle \text{grad } f(p), \dot{\gamma}(0) \rangle \geq -\|\text{grad } f(p)\|.$$

By the assumed lower bound on τ , one has $\mu(p, \tau) > 2\|\text{grad } f(p)\|/r_p$, and therefore

$$\varphi'(r_p) > -\|\text{grad } f(p)\| + 2\|\text{grad } f(p)\| = \|\text{grad } f(p)\| > 0.$$

Thus moving slightly inward from z along γ decreases Φ_p , contradicting the minimality of z . Hence, the unique minimizer lies in $B_{r_p}(p)$. \square

Lemma 5.6. *Let Assumptions 1, 2, 3, and 4 hold. Fix $\underline{r} > 0$, $\theta \in (0, 1)$, and $\eta_0 > 0$. For each $y \in \text{int}(\mathcal{M}_{\text{ex}})$ satisfying $\text{dist}(y, \partial\mathcal{M}_{\text{ex}}) \geq \underline{r}$, define*

$$r(y) \triangleq \min\left\{\theta \text{dist}(y, \partial\mathcal{M}_{\text{ex}}), \rho\right\}, \quad \delta(y) \triangleq \delta_+(r(y)), \quad \text{and}$$

$$\tau(y) \triangleq \max\left\{\frac{L_{\log}^{\pm}(r(y))\|\text{grad } h(y)\| - 2w_+(x)\delta_{\text{ex}}}{\delta(y)} + \frac{2\|\text{grad } f(y)\|}{\delta(y)r(y)} + \eta_0, 1 - 2w_-(x)\delta_{\text{ex}}, 1\right\}.$$

Then there exists a constant $\bar{\tau} < \infty$ such that $\tau(y) \leq \bar{\tau}$ for every such y .

Proof. Since \mathcal{M}_{ex} is compact and f, h are smooth on \mathcal{M}_{ex} ,

$$G_f \triangleq \sup_{z \in \mathcal{M}_{\text{ex}}} \|\text{grad } f(z)\| < \infty, \quad G_h \triangleq \sup_{z \in \mathcal{M}_{\text{ex}}} \|\text{grad } h(z)\| < \infty.$$

Moreover, $r_\theta \triangleq \min\{\theta r, \rho\} \leq r(y) \leq \rho$. Since $\rho < \pi/(2\sqrt{\Lambda_+})$ and δ_+ is decreasing,

$$\delta_y \triangleq \delta_+(r(y)) \geq \delta_+(\rho) =: \underline{\delta} > 0.$$

Also L_{\log}^{\pm} is continuous and nondecreasing on $[0, \rho]$, so $L_{\log}^{\pm}(r(y)) \leq L_{\log}^{\pm}(\rho) =: \bar{L}_{\log}$. Therefore,

$$\frac{L_{\log}^{\pm}(r(y))\|\text{grad } h(y)\| - 2w_+(x)\delta_{\text{ex}}}{\delta_y} + \frac{2\|\text{grad } f(y)\|}{\delta_y r(y)} + \eta_0 \leq \frac{\bar{L}_{\log} G_h - 2w_+(x)\delta_{\text{ex}}}{\underline{\delta}} + \frac{2G_f}{\underline{\delta} r_\theta} + \eta_0.$$

Hence $\tau(y) \leq \max\left\{\frac{\bar{L}_{\log} G_h - 2w_+(x)\delta_{\text{ex}}}{\underline{\delta}} + \frac{2G_f}{\underline{\delta} r_\theta} + \eta_0, 1 - 2w_-(x)\delta_{\text{ex}}, 1\right\} =: \bar{\tau} < \infty$. \square

5.2 Proof of Theorem 4.4

With the strong convexity of the local model and the invariance of the proximal step established, each subproblem is well posed, each accepted step yields a quantitative decrease, and the summability of the step sizes implies stationarity of every accumulation point.

Proof. Set $\mathcal{S}_0 \triangleq \{y \in \mathcal{M}_{\text{ex}} : f(y, x) \leq f(y_0, x)\}$. Since $f(\cdot, x)$ is continuous on \mathcal{M}_{ex} , the set \mathcal{S}_0 is compact. Moreover, by the hypothesis $f(y_0, x) < \min_{y \in \partial \mathcal{M}_{\text{ex}}} f(y, x)$, we have $\mathcal{S}_0 \cap \partial \mathcal{M}_{\text{ex}} = \emptyset$, and therefore $\underline{r} \triangleq \text{dist}(\mathcal{S}_0, \partial \mathcal{M}_{\text{ex}}) > 0$.

Since $r_k < \text{dist}(y_k, \partial \mathcal{M}_{\text{ex}})$, one has $\mathcal{M}_k \subset \mathcal{M}_{\text{ex}}$. By Proposition 5.4, each model function Φ_k is strongly geodesically convex on \mathcal{M}_k . Hence, in the exact case, the subproblem has a unique minimizer, and Lemma 5.5 implies that this minimizer belongs to $B_{r_k}(y_k) \subset \mathcal{M}_{\text{ex}}$. In the inexact case, the algorithm chooses $y_{k+1} \in \mathcal{M}_k \subset \mathcal{M}_{\text{ex}}$ by construction. Thus, in both cases, $y_{k+1} \in \mathcal{M}_{\text{ex}}$. Now, let $d_k \triangleq d(y_k, y_{k+1})$, and derive the descent estimates. In the exact method, $\Phi_k(y_{k+1}) \leq \Phi_k(y_k)$, so

$$g(y_k) - g(y_{k+1}) + \langle \text{grad } h(y_k), \log_{y_k}(y_{k+1}) \rangle \geq (\tau_k/2) d_k^2.$$

Since $y_k, y_{k+1} \in \mathcal{M}_k$, Lemma 5.2 applies along their minimizing geodesic,

$$h(y_{k+1}) - h(y_k) \geq \langle \text{grad } h(y_k), \log_{y_k}(y_{k+1}) \rangle + w_-(x) \delta_{\text{ex}} d_k^2.$$

Adding the two inequalities yields $f(y_k, x) - f(y_{k+1}, x) \geq (\tau_k/2 + w_-(x) \delta_{\text{ex}}) d_k^2$. Since $\tau_k \geq 1 - 2w_-(x) \delta_{\text{ex}}$, we obtain

$$f(y_{k+1}, x) \leq f(y_k, x) - (1/2) d_k^2. \quad (8)$$

For the inexact method, geodesic convexity of Φ_k on \mathcal{M}_k gives

$$\Phi_k(y_k) - \Phi_k(y_{k+1}) \geq \left\langle \text{grad } \Phi_k(y_{k+1}), \log_{y_{k+1}}(y_k) \right\rangle.$$

Hence $\Phi_k(y_k) - \Phi_k(y_{k+1}) \geq -\|\text{grad } \Phi_k(y_{k+1})\| d_k$. By the stopping rule,

$$\|\text{grad } \Phi_k(y_{k+1})\| \leq \min(\varepsilon_k, \zeta d_k) \leq \zeta d_k, \text{ so } \Phi_k(y_k) - \Phi_k(y_{k+1}) \geq -\zeta d_k^2.$$

Expanding Φ_k and using again the lower second-order bound for h from Lemma 5.2,

$$f(y_k, x) - f(y_{k+1}, x) \geq (\tau_k/2 + w_-(x) \delta_{\text{ex}} - \zeta) d_k^2.$$

Since $\tau_k \geq 1 - 2w_-(x) \delta_{\text{ex}}$ and $\zeta = 1/4$, it follows that

$$f(y_{k+1}, x) \leq f(y_k, x) - (1/4) d_k^2. \quad (9)$$

In either case, $f(y_{k+1}, x) \leq f(y_k, x)$. By induction, $y_k \in \mathcal{S}_0$, for $k \geq 0$. Therefore, $\text{dist}(y_k, \partial \mathcal{M}_{\text{ex}}) \geq \underline{r}$, for $k \geq 0$. Lemma 5.6 then yields $\sup_{k \geq 0} \tau_k < \infty$.

Summing (8) or (9) from $k = 0$ to N proves (7)

$$\kappa \sum_{k=0}^N d_k^2 \leq f(y_0, x) - f(y_{N+1}, x) \leq f(y_0, x) - f_*, \quad \min_{0 \leq k \leq N} d_k^2 \leq \frac{1}{N+1} \sum_{k=0}^N d_k^2 \leq \frac{f(y_0, x) - f_*}{\kappa(N+1)}$$

In particular, $\sum_{k=0}^{\infty} d_k^2 < \infty$, so $d_k \rightarrow 0$. Since $\{y_k\} \subset \mathcal{S}_0$ and \mathcal{S}_0 is compact, the sequence has at least one accumulation point $\bar{y} \in \mathcal{S}_0 \subset \mathcal{M}_{\text{ex}}$. This proves (1).

Next we show stationarity. Let \bar{y} be an accumulation point and take $y_{k_j} \rightarrow \bar{y}$. Since $d_{k_j} \rightarrow 0$, also $y_{k_j+1} \rightarrow \bar{y}$. Writing $(d \log_{y_k})_{y_{k+1}}^* : T_{y_k} \Omega \rightarrow T_{y_{k+1}} \Omega$ for the adjoint of $d(\log_{y_k})_{y_{k+1}}$, define the residual

$$e_k \triangleq \text{grad } \Phi_k(y_{k+1}) = \text{grad } g(y_{k+1}) - (d \log_{y_k})_{y_{k+1}}^* \text{grad } h(y_k) - \tau_k \log_{y_{k+1}}(y_k).$$

In the exact case, $e_k = 0$. In the inexact case, $\|e_k\| = \|\text{grad } \Phi_k(y_{k+1})\| \leq \varepsilon_k \rightarrow 0$, since $\sum_{k=0}^{\infty} \varepsilon_k < \infty$. Because $\bar{y} \in \text{int}(\mathcal{M}_{\text{ex}})$ and $y_{k_j}, y_{k_j+1} \rightarrow \bar{y}$, for j large enough the points y_{k_j} and y_{k_j+1} lie in a common normal neighborhood of \bar{y} . Let $P_j : T_{y_{k_j}} \Omega \rightarrow T_{\bar{y}} \Omega$, $Q_j : T_{y_{k_j+1}} \Omega \rightarrow T_{\bar{y}} \Omega$ be parallel transport along the corresponding minimizing geodesics, and define $\mathcal{A}_j \triangleq Q_j (d \log_{y_{k_j}})_{y_{k_j+1}}^* P_j^{-1}$ on $T_{\bar{y}} \Omega$. Applying Q_j to the identity defining e_{k_j} , we obtain

$$Q_j e_{k_j} = Q_j \text{grad } g(y_{k_j+1}) - \mathcal{A}_j (P_j \text{grad } h(y_{k_j})) - \tau_{k_j} Q_j \log_{y_{k_j+1}}(y_{k_j}).$$

Since g and h are smooth on \mathcal{M}_{ex} ,

$$Q_j \text{grad } g(y_{k_j+1}) \rightarrow \text{grad } g(\bar{y}), \quad P_j \text{grad } h(y_{k_j}) \rightarrow \text{grad } h(\bar{y}).$$

Moreover, on a common normal neighborhood of the diagonal, $(p, y) \mapsto (d \log_p)_y^*$ is smooth, so $\mathcal{A}_j \rightarrow \text{Id}_{T_{\bar{y}} \Omega}$ in operator norm. Finally,

$$\|\tau_{k_j} Q_j \log_{y_{k_j+1}}(y_{k_j})\| = \tau_{k_j} d(y_{k_j+1}, y_{k_j}) \leq \left(\sup_{k \geq 0} \tau_k \right) d_{k_j} \rightarrow 0.$$

Since $\|Q_j e_{k_j}\| = \|e_{k_j}\| \rightarrow 0$, passing to the limit gives

$$0 = \text{grad } g(\bar{y}) - \text{grad } h(\bar{y}) = \text{grad } f(\bar{y}, x).$$

Thus every accumulation point is stationary, proving (2). \square

6 Improved rates on real-analytic manifolds

The previous section established descent of the objective and stationarity of all accumulation points of the proximal DC iterates. In this section, we show that these qualitative conclusions can be sharpened when the ambient manifold is real analytic. Indeed, on $\text{int}(\mathcal{M}_{\text{ex}})$ the objective $f(\cdot, x)$ is real analytic and therefore satisfies a Kurdyka–Łojasiewicz inequality near its stationary points. Combined with the descent and relative-error estimates for the proximal scheme, this yields convergence of the whole sequence, with corresponding finite, linear, or sublinear rates determined by the KL exponent.

Assumption 5. The ambient Riemannian manifold (Ω, d) is real analytic.

Corollary 6.1. *Let Assumptions 1, 2, 3, and 5 hold. Fix $x \in \mathbb{R}^q$. Then the function $f(\cdot, x)$ in (5) is real analytic on $\text{int}(\mathcal{M}_{\text{ex}})$. Consequently, for every $\bar{y} \in \text{int}(\mathcal{M}_{\text{ex}})$, the function $f(\cdot, x)$ satisfies the Riemannian Kurdyka–Łojasiewicz property at \bar{y} . More precisely, there exist a neighborhood U of \bar{y} , constants $c > 0$, $\vartheta \in [0, 1)$, and $\delta > 0$ such that*

$$\|\text{grad } f(y, x)\| \geq c |f(y, x) - f(\bar{y}, x)|^{\vartheta}, \quad y \in U, |f(y, x) - f(\bar{y}, x)| < \delta. \quad (10)$$

Equivalently, the KL inequality holds at \bar{y} with $\varphi(s) = (1/c(1 - \vartheta)) s^{1-\vartheta}$, for $s \in [0, \delta)$.

Proof. Fix $i \in \{1, \dots, m\}$. Since $y_i \in \overline{B_r(c)}$ and $y \in \mathcal{M}_{\text{ex}}$, it is implied that

$$d(y_i, y) \leq r + \rho_{\text{ex}} < \iota_{r,c} \leq \text{inj}_\Omega(y_i),$$

the point y lies in the injectivity ball of y_i . Because (Ω, d) is real analytic, the map \exp_{y_i} is real analytic on a neighborhood of $0 \in T_{y_i}\Omega$, hence its local inverse \log_{y_i} is real analytic on $\text{int}(\mathcal{M}_{\text{ex}})$. Therefore $y \mapsto d^2(y_i, y) = \|\log_{y_i}(y)\|_{y_i}^2$ is real analytic on $\text{int}(\mathcal{M}_{\text{ex}})$. Since $f(\cdot, x)$ is a finite linear combination of these squared-distance terms, it is real analytic on $\text{int}(\mathcal{M}_{\text{ex}})$.

Now choose a real-analytic chart $\psi : U_0 \rightarrow V_0 \subset \mathbb{R}^n$ around \bar{y} , set $\bar{z} \triangleq \psi(\bar{y})$, and define $\tilde{f} \triangleq f \circ \psi^{-1}$. Then \tilde{f} is real analytic on V_0 . By the classical Łojasiewicz gradient inequality in Euclidean space, there exists a neighborhood $V \subset V_0$ of \bar{z} , constants $c_0 > 0$, $\vartheta \in [0, 1)$, and $\delta > 0$ such that

$$\|\nabla \tilde{f}(z)\| \geq c_0 |\tilde{f}(z) - \tilde{f}(\bar{z})|^\vartheta, \quad z \in V, |\tilde{f}(z) - \tilde{f}(\bar{z})| < \delta.$$

Shrinking $U \triangleq \psi^{-1}(V)$ if necessary, the Euclidean norm of $\nabla \tilde{f}$ and the Riemannian norm of $\text{grad } f$ are equivalent on U , so there exists $c > 0$ such that (10) holds. This is exactly the KL property with the displayed power-type desingularizing function. \square

Lemma 6.2. *Let Assumptions 1–5 hold, and let $d_k \triangleq d(y_k, y_{k+1})$. Then there exists a constant $C_{\text{rel}} > 0$ such that $\|\text{grad } f(y_{k+1}, x)\| \leq C_{\text{rel}} d_k$ for all sufficiently large k . More precisely, one may take*

$$C_{\text{rel}} = \begin{cases} L_A G_h + L_h + \bar{\tau}, & \text{exact step,} \\ L_A G_h + L_h + \bar{\tau} + \zeta, & \text{inexact step,} \end{cases}$$

where $G_h \triangleq \sup_{z \in \mathcal{M}_{\text{ex}}} \|\text{grad } h(z)\|$, $\bar{\tau}$ is the uniform bound from Lemma 5.6, and $L_A, L_h > 0$ are the local Lipschitz constants defined as $L_A = L_{\log}^\pm(\rho)$, $L_h \leq 2w_-(x)\zeta_{\text{ex}}$.

Proof. By the proof of Theorem 4.4, all iterates belong to the compact strict sublevel set

$$\mathcal{S}_0 \triangleq \{y \in M_{\text{ex}} : f(y, x) \leq f(y_0, x)\} \subset \text{int}(\mathcal{M}_{\text{ex}}),$$

and Lemma 5.6 gives $\tau_k \leq \bar{\tau}$ for all k . Since h is smooth on the compact set \mathcal{M}_{ex} , we also have $G_h < \infty$.

Let $\mathcal{D}_\rho \triangleq \{(p, y) \in M_{\text{ex}} \times M_{\text{ex}} : d(p, y) \leq \rho\}$. For $(p, y) \in \mathcal{D}_\rho$, define

$$A(p, y) \triangleq (d_y \log_p)^* : T_p\Omega \rightarrow T_y\Omega.$$

Since the pairs in \mathcal{D}_ρ lie in a common normal neighborhood, A is well defined and smooth on \mathcal{D}_ρ . For $A(p, y) \triangleq (d_y \log_p)^*$ and $\psi_\xi(z) \triangleq \langle \xi, \log_p(z) \rangle_p$, let γ be the unit-speed minimizing geodesic from p to y . Then, for any unit parallel field V along γ ,

$$\langle A(p, y)\xi - P_{p \rightarrow y}\xi, V_y \rangle_y = \int_0^{d(p,y)} \text{Hess}_{\gamma(s)} \psi_\xi(\dot{\gamma}(s), V(s)) ds.$$

Hence Lemma 5.1 gives $\|A(p, y)\xi - P_{p \rightarrow y}\xi\| \leq L_A \|\xi\| d(p, y)$ with $L_A \triangleq L_{\log}^\pm(\rho)$. Also, by Lemma 5.2, h is L_h -smooth on M_{ex} , with $L_h \leq 2w_-(x)\zeta_{\text{ex}}$. Therefore,

$$\begin{aligned} & \|A(p, y) \text{grad } h(p) - \text{grad } h(y)\| \\ & \leq \|A(p, y) \text{grad } h(p) - P_{p \rightarrow y} \text{grad } h(p)\| + \|P_{p \rightarrow y} \text{grad } h(p) - \text{grad } h(y)\| \\ & \leq (L_A G_h + L_h) d(p, y), \quad (p, y) \in \mathcal{D}_\rho. \end{aligned} \tag{11}$$

Now $y_{k+1} \in \mathcal{M}_k \subset \overline{B_\rho(y_k)}$, so $(y_k, y_{k+1}) \in \mathcal{D}_\rho$. For the exact step,

$$0 = \text{grad } g(y_{k+1}) - A(y_k, y_{k+1}) \text{grad } h(y_k) - \tau_k \log_{y_{k+1}}(y_k).$$

Hence, using (11),

$$\begin{aligned} \|\text{grad } f(y_{k+1}, x)\| &= \|\text{grad } g(y_{k+1}) - \text{grad } h(y_{k+1})\| \\ &\leq \|A(y_k, y_{k+1}) \text{grad } h(y_k) - \text{grad } h(y_{k+1})\| + \tau_k \|\log_{y_{k+1}}(y_k)\| \\ &\leq (L_A G_h + L_h + \bar{\tau}) d_k. \end{aligned}$$

For the inexact step, let $r_k \triangleq \text{grad } \Phi_k(y_{k+1})$.

Then $\|r_k\| \leq \min\{\varepsilon_k, \zeta d_k\} \leq \zeta d_k$, and $r_k = \text{grad } g(y_{k+1}) - A(y_k, y_{k+1}) \text{grad } h(y_k) - \tau_k \log_{y_{k+1}}(y_k)$.

Therefore,

$$\begin{aligned} \|\text{grad } f(y_{k+1}, x)\| &\leq \|r_k\| + \|A(y_k, y_{k+1}) \text{grad } h(y_k) - \text{grad } h(y_{k+1})\| + \tau_k \|\log_{y_{k+1}}(y_k)\| \\ &\leq (L_A G_h + L_h + \bar{\tau} + \zeta) d_k. \end{aligned}$$

□

Theorem 6.3. *Let Assumptions 1–5 hold. Let $\{y_k\} \subset \mathcal{M}_{\text{ex}}$ be the sequence generated by Algorithm 1, and define*

$$S \triangleq \left\{ \bar{y} \in \mathcal{M}_{\text{ex}} : \exists k_j \rightarrow \infty \text{ with } y_{k_j} \rightarrow \bar{y} \right\}, \quad d_k \triangleq d(y_k, y_{k+1}).$$

Then $S = \{y_\star\}$ for some stationary point y_\star of $f(\cdot, x)$, and therefore $y_k \rightarrow y_\star$. Moreover, if $\vartheta \in [0, 1)$ is a KL exponent of $f(\cdot, x)$ at y_\star , then:

- *if $\vartheta = 0$, the sequence converges in finite time;*
- *if $\vartheta \in (0, 1/2]$, then $d(y_k, y_\star) = \mathcal{O}(\rho^k)$ for some $\rho \in (0, 1)$;*
- *if $\vartheta \in (1/2, 1)$, then $d(y_k, y_\star) = \mathcal{O}(k^{-\frac{1-\vartheta}{2\vartheta-1}})$.*

Proof. Set $f_k \triangleq f(y_k, x)$. By the proof of Theorem 4.4, for every $k \geq 0$

$$f_k - f_{k+1} \geq \kappa d_k^2. \tag{12}$$

Hence $\{f_k\}$ is nonincreasing. Since f is continuous on the compact set \mathcal{M}_{ex} , it is bounded below there, and thus $f_k \downarrow \ell$ for some $\ell \in \mathbb{R}$. Again by Theorem 4.4, every cluster point of $\{y_k\}$ is stationary for $f(\cdot, x)$, and $\{y_k\} \subset \mathcal{S}_0 \subset \text{int}(\mathcal{M}_{\text{ex}})$, where \mathcal{S}_0 is the compact strict sublevel set introduced in the proof of Theorem 4.4. The cluster set S is nonempty and compact. If $\bar{y} \in S$, there exists a subsequence $y_{k_j} \rightarrow \bar{y}$, hence by continuity $f(\bar{y}, x) = \lim_j f_{k_j} = \ell$. Therefore $f(\cdot, x)$ is constant on S .

By Corollary 6.1, $f(\cdot, x)$ satisfies the KL property at every point of S . Since S is compact and $f \rightarrow \ell$ on S , the standard uniformized KL lemma yields $\varepsilon > 0$, $\eta > 0$, and a concave function $\varphi : [0, \eta) \rightarrow [0, \infty)$ such that

$$\varphi'(f(y, x) - \ell) \|\text{grad } f(y, x)\| \geq 1 \tag{13}$$

whenever $\text{dist}(y, S) < \varepsilon$ and $\ell < f(y, x) < \ell + \eta$. Because $\{y_k\}$ is contained in the compact set \mathcal{S}_0 , one has $\text{dist}(y_k, S) \rightarrow 0$; otherwise a subsequence staying a fixed positive distance from S would admit a further convergent subsequence with limit in S , a contradiction. Since also $f_k \rightarrow \ell$, estimate (13) holds at y_k for all large enough k .

Now reindex Lemma 6.2 to obtain a constant $C_{\text{rel}} > 0$ such that

$$\|\text{grad } f(y_k, x)\| \leq C_{\text{rel}} d_{k-1} \tag{14}$$

for all sufficiently large k . By concavity of φ ,

$$\varphi(f_k - \ell) - \varphi(f_{k+1} - \ell) \geq \varphi'(f_k - \ell)(f_k - f_{k+1}).$$

Combining this with (13), (12), and (14), we obtain, for all large enough k ,

$$\varphi(f_k - \ell) - \varphi(f_{k+1} - \ell) \geq \frac{f_k - f_{k+1}}{\|\text{grad } f(y_k, x)\|} \geq \frac{\kappa}{C_{\text{rel}}} \frac{d_k^2}{d_{k-1}}.$$

Hence $d_k \leq (1/2)d_{k-1} + (C_{\text{rel}}/2\kappa)(\varphi(f_k - \ell) - \varphi(f_{k+1} - \ell))$. Summing this inequality from $k = k_0 + 1$ to N , where k_0 is large enough for all previous estimates to hold, gives

$$\frac{1}{2} \sum_{k=k_0+1}^{N-1} d_k + d_N \leq \frac{1}{2}d_{k_0} + \frac{C_{\text{rel}}}{2\kappa} \varphi(f_{k_0+1} - \ell).$$

Therefore $\sum_{k=0}^{\infty} d_k < \infty$. The sequence has finite length, so it is Cauchy and, since \mathcal{M}_{ex} is compact, there exists $y_\star \in \mathcal{M}_{\text{ex}}$ such that $y_k \rightarrow y_\star$. Hence $S = \{y_\star\}$. As every cluster point is stationary by Theorem 4.4, we also have $\text{grad } f(y_\star, x) = 0$.

It remains to derive the rates. By Corollary 6.1, there exist a neighborhood U of y_\star , constants $c > 0$, $\vartheta \in [0, 1)$, and $\delta > 0$ such that

$$\|\text{grad } f(y, x)\| \geq c |f(y, x) - f(y_\star, x)|^\vartheta, \quad y \in U, \quad |f(y, x) - f(y_\star, x)| < \delta.$$

Choose a real-analytic chart $\psi : U \rightarrow V \subset \mathbb{R}^n$ around y_\star , set $z_k \triangleq \psi(y_k)$ and $\tilde{f} \triangleq f \circ \psi^{-1}$. After shrinking U if necessary, the chart and its inverse are bi-Lipschitz on U , and the Euclidean and Riemannian gradient norms are uniformly equivalent there. Consequently, for all large enough k ,

$$\tilde{f}(z_k) - \tilde{f}(z_{k+1}) \geq a \|z_{k+1} - z_k\|^2, \quad \|\nabla \tilde{f}(z_k)\| \leq b \|z_k - z_{k-1}\|$$

for some constants $a, b > 0$. Thus the charted sequence $\{z_k\}$ satisfies the standard Euclidean sufficient-decrease and relative-error conditions, and the classical KL rate theorem (see, e.g., [3, Theorem 2]) applies to \tilde{f} at $z_\star \triangleq \psi(y_\star)$. Therefore:

- if $\vartheta = 0$, then z_k (and hence y_k) is eventually constant;
- if $\vartheta \in (0, 1/2]$, then z_k converges R -linearly to z_\star ;
- if $\vartheta \in (1/2, 1)$, then $\|z_k - z_\star\| = \mathcal{O}(k^{-\frac{1-\vartheta}{2\vartheta-1}})$.

Since the chart is bi-Lipschitz, the same rate statements hold for $d(y_k, y_\star)$. □

7 Numerical Analysis

In this section, we provide numerical examples to illustrate the efficiency of our approach. In addition to global FRIDA, we also test local FRIDA, as defined in Remark 3.1.

7.1 Regression on the Sphere

We consider Fréchet regression with predictor $X \in \mathbb{R}$ and response $Y \in S^2$, where $S^2 = \{x \in \mathbb{R}^3 : \|x\| = 1\}$, with tangent space at p defined as $T_p S^2 = \{v \in \mathbb{R}^3 : \langle v, p \rangle = 0\}$, and geodesic distance $d(x, y) = \arccos(\langle x, y \rangle)$.

7.1.1 Regression on Geodesic Data

For illustration, we first consider a simple case with three responses on a common geodesic segment of S^2 , with predictors $\{0, 0.5, 1\}$ and responses $\{y_0, y_{0.5}, y_1\}$. We choose an extrapolating test predictor $x_{\text{test}} = 1.87$, which lies outside the sufficient predictor region where our theory guarantees interiority of minimizers. Nevertheless, the objective is well defined on the chosen normal ball, and a minimizer is observed numerically in this example. Thus, this experiment stress-tests Algorithm 1 beyond the conservative sufficient safe-region condition. Figure 2(a)–(b) shows the weighted Fréchet objective on S^2 . Panel (a)

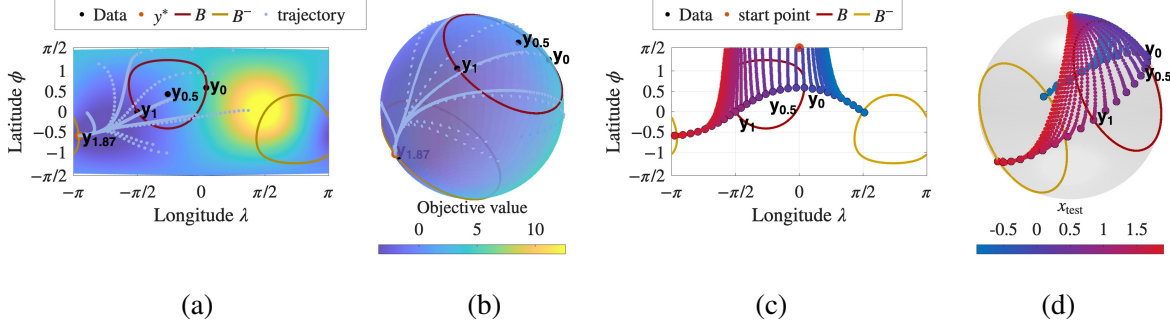


Figure 2: Global Fréchet Regression on data lying on a geodesic of S^2 . Panels (a)–(b) show the weighted Fréchet objective $f(\cdot, x)$ in longitude–latitude coordinates and on the sphere. Black points are the data $\{y_0, y_{0.5}, y_1\}$, the orange point is a stationary point, the light blue curves are trajectories from random initializations, and the red and gold curves denote the boundaries of B and B^- . Panels (c)–(d) show the geodesic regression with various x_{test} . The red dot is the start point. The color of the trajectories is proportional to x_{test} .

gives the longitude–latitude projection, and Panel (b) shows the corresponding visualization on the sphere. The black data points correspond to $\{y_0, y_{0.5}, y_1\}$, and the orange point marks a stationary point. The light blue curves are trajectories generated by Algorithm 1 from random initializations. The red and gold curves denote the boundaries of the geodesic ball $B \subset \mathcal{M}_r$ and its antipodal counterpart B^- , respectively. The color map represents the functional value $f(\cdot, x)$. In both views, the trajectories from different initial points converge to the same stationary point, indicating the stability of the proposed method in the selected region.

Additionally, under the same setup, we test Algorithm 1 when finding the response y corresponding to different predictors x varying over $[-0.9, 1.9]$ with a fixed initialization point.

Figure 2(c)–(d) shows the geodesic regression experiment with several test predictor values x_{test} . Panel (c) gives the longitude–latitude projection, and Panel (d) shows the corresponding visualization on the sphere. The red dot marks the start point, and the color of each trajectory corresponds to the value of x_{test} . In both views, the estimated points converge to stationary points of the corresponding weighted Fréchet objectives, showing that the method consistently identifies the regression estimates across different test predictor values.

For the next illustration, we add noise under the same geodesic ground-truth configuration as in the previous experiments. The predictors are sampled at 20 equally spaced values in $[0, 1]$, and the corresponding responses are the 20 points along the geodesic at those values. To generate noisy observations, for each response point $y_i \in S^2$, we sample a Gaussian vector $z_i \in \mathbb{R}^3$, project it onto the tangent space $T_{y_i} S^2$, scale the projected vector by a noise level parameter $\sigma = 0.1$, and map it back to the sphere using the exponential map. The resulting observations are $Y_i = \exp_{y_i}(v_i)$, and $v_i = \sigma(z_i - \langle z_i, y_i \rangle y_i)$, where $z_i \sim \mathcal{N}(0, I_3)$. Figure 3 (a)–(b) shows the noisy geodesic regression experiment on S^2 . Panel (a) gives the longitude–latitude projection, and Panel (b) shows the corresponding visualization on the sphere. The true geodesic

curve is plotted in blue, the DCA regression estimate is shown in orange, and the noisy manifold-valued observations are displayed in green. The initialization point is marked by a purple star. In both views, the estimated curve closely follows the underlying geodesic despite the intrinsic noise in the observations, indicating that the regression procedure recovers the main geodesic structure of the data.

7.1.2 Regression on Spiral Data

We next consider a spherical regression example with a ground-truth curve

$$m(x) = \left(\sqrt{1-x^2} \cos(\pi x), \sqrt{1-x^2} \sin(\pi x), x \right), \quad x \in (0, 1),$$

which forms a spiral-like path on S^2 . Observations are generated by adding tangent-space noise at $m(X_i)$ and mapping back to the sphere using the exponential map. We then compare local and global Fréchet regression fits.

Figure 3(c)–(d) shows the spiral-noise experiment on S^2 . Panel (c) gives the longitude–latitude projection, and Panel (d) maps the same curves onto the sphere. The true spiral response is shown in blue, the local Fréchet estimate in orange, and the global Fréchet estimate in purple. Noisy observations are plotted in green, and the initialization is marked by a star. Compared with the global estimator, the local estimator follows the spiral more closely and captures its local variation, while the global estimator recovers the overall trend but smooths out part of the local geometric structure.

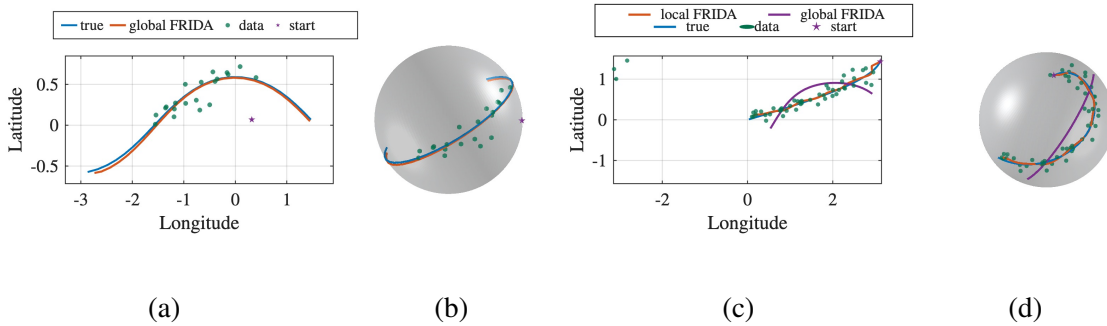


Figure 3: Fréchet regression on noisy data on S^2 . Panels (a)–(b) show global Fréchet regression for noisy observations lying near a geodesic, in longitude–latitude coordinates and on the 3D sphere, respectively. Panels (c)–(d) compare local and global Fréchet regression for spiral-noise data in the same two views. Blue denotes the true curve, green the noisy observations, orange the FRIDA local estimate, and purple the global estimate or initialization point. The estimates recover the main spherical regression structure despite the presence of intrinsic noise.

7.2 Comparison with GD on $S^2 \times S^1$

We generate synthetic responses on the product manifold $\mathcal{M} = S^2 \times S^1$, writing each response as $y = (p, \theta)$, with $p \in S^2 \subset \mathbb{R}^3$ and $\theta \in [0, 2\pi)$. We use the product metric $g_{\mathcal{M}} = g_{S^2}^{\text{round}} \oplus g_{S^1}^{\text{flat}}$, where the two factors carry the standard round and angular metrics.

We take $n = 40$ equally spaced predictors $x_i \in [0, 1]$. The noiseless regression function starts from $y_{\text{base}} = ((0, 0, 1), 0)$.

Its spherical component moves from the north pole in the tangent direction $e = (1, 0, 0) \in T_{(0,0,1)}S^2$, and its circular component evolves on S^1 . Using $\alpha(x) = 1.40(3x^2 - 2x^3)$, which smooths the spherical motion near the endpoints, we define $m(x) = \left((\sin \alpha(x), 0, \cos \alpha(x)), 0.80\pi x \bmod 2\pi \right)$, for $x \in [0, 1]$. Since

$\max_x \alpha(x) = 1.40 < \pi/2$, the noiseless spherical component remains in the open hemisphere centered at $(0, 0, 1)$.

Intrinsic noise is added independently to each factor. On S^2 , a Gaussian vector in \mathbb{R}^3 is projected onto $T_{p_{\text{true}}(x_i)}S^2$, normalized, scaled by a Gaussian amplitude with standard deviation $\sigma_{S^2} = 0.045$, and mapped back by the exponential map. On S^1 , Gaussian angular noise with standard deviation $\sigma_{S^1} = 0.035$ is added. This gives noisy responses $y_i = (p_i, \theta_i) \in S^2 \times S^1$. The product manifold satisfies $0 \leq K \leq 1$, and along the chosen regression curve, the effective curvature is bounded above by approximately 0.41.

For the optimization comparison, we keep only the test predictors x_{test} whose global Fréchet regression weights contain at least one negative value. For each such x_{test} , GD and FRIDA solve the weighted Fréchet problem from the same noisy response. GD uses at most 500 iterations, while FRIDA uses at most 500 outer iterations and 1000 inner iterations per subproblem, with all gradient tolerances set to 10^{-8} . We report the final objective value, outer iteration counts, FRIDA inner iteration counts, and the final and best gradient norms.

Figure 4(a) summarizes the GD–FRIDA comparison over test predictors x_{test} whose global weights include negative values. The four panels report the best Riemannian gradient norm $\min_k \|\text{grad } F(y_k)\|$, final objective value, outer iteration count, and FRIDA inner iteration count. FRIDA typically achieves lower gradient norms and requires far fewer outer iterations than GD, while both methods achieve nearly identical final objective values. The FRIDA inner counts remain well below the prescribed limit. Figure 4(b) shows representative convergence trajectories. For readability, the gradient-norm Panel shows only the first 100 GD iterations, together with the full FRIDA trajectory. FRIDA reaches a small gradient norm much faster than GD. The objective-value Panel shows that both methods decrease the objective and converge to the same final value, with the displayed final values agreeing with the shown precision.

Remark 7.1 (Why FRIDA can outperform gradient descent). FRIDA is not uniformly better than gradient descent for all nonconvex problems, but it is well suited to the weighted Fréchet objective considered here. While GD uses only first-order information from the full objective F and may need small steps in ill-conditioned signed-distance landscapes, FRIDA exploits the decomposition $F = g - h$. By linearizing $-h$ and minimizing a locally convex surrogate involving g , each FRIDA update can make more structured progress than a single gradient step.

7.3 Spiral Regression on the Torus

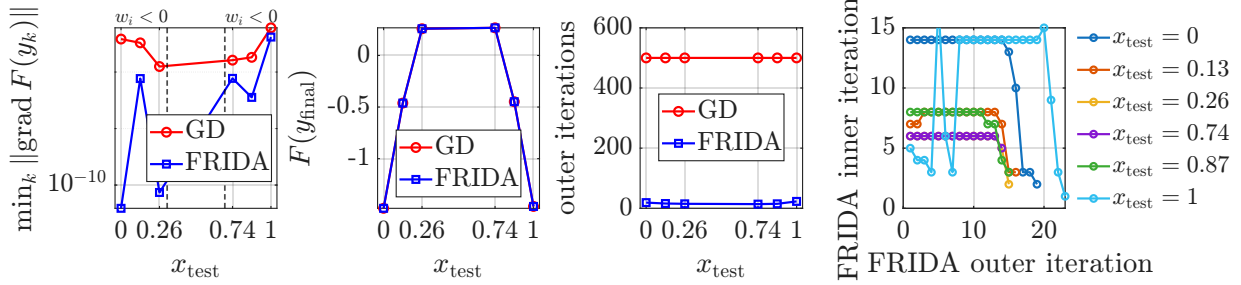
In the final experiment, we consider regression on an embedded torus with angular coordinates $(\theta, \phi) \in S^1 \times S^1$, where θ parametrizes the central circle and ϕ the cross-sectional circle. For major radius R and minor radius r , we use $F(\theta, \phi) = ((R + r \cos \phi) \cos \theta, (R + r \cos \phi) \sin \theta, r \sin \phi)$, whose induced metric is $ds^2 = (R + r \cos \phi)^2 d\theta^2 + r^2 d\phi^2$. Thus, motion in the θ -direction is scaled by $R + r \cos \phi$, while motion in the ϕ -direction is scaled by r .

The sectional curvature is $K(\phi) = \frac{\cos \phi}{r(R+r \cos \phi)}$. Hence, the outer region has positive curvature, the inner region has negative curvature, and the transition regions near $\phi = \pi/2$ and $\phi = 3\pi/2$ have curvature close to zero.

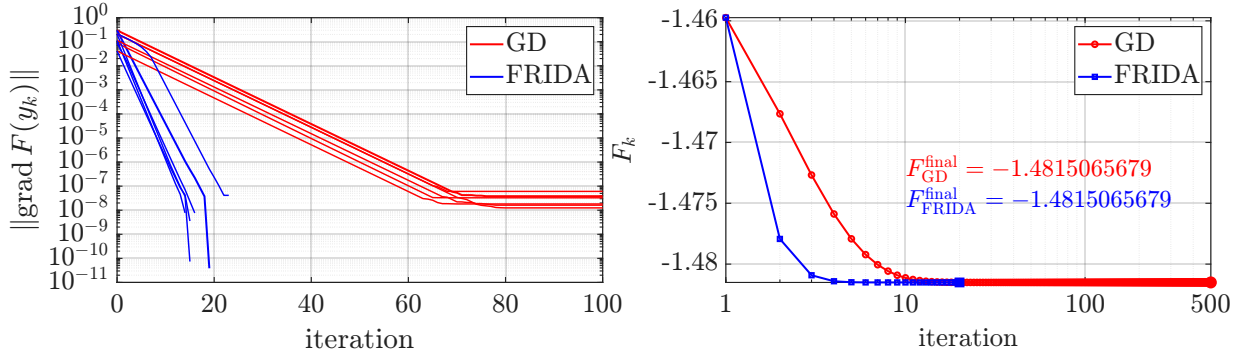
Unlike the sphere experiment, the torus experiment uses approximate local geometry, since exact intrinsic operations on the embedded torus generally require geodesic boundary-value solves [13]. We work in a small angular patch inside the normal/convexity regime, where squared distances are smooth and locally convex, metric variation is mild, and wrapping or cut-locus effects are avoided. We approximate

$$d^2((\theta_1, \phi_1), (\theta_2, \phi_2)) \approx (R + r \cos \phi_{\text{mid}})^2 (\theta_1 - \theta_2)^2 + r^2 (\phi_1 - \phi_2)^2,$$

where ϕ_{mid} is the midpoint angular coordinate, and use the associated local orthonormal frame for logarithm/exponential maps. This matches the metric quadratic approximation to squared geodesic distance



(a) Summary of selected test predictors with negative global weights. From left to right, the Panels report the best Riemannian gradient norm, final objective value, number of outer iterations, and FRIDA inner iteration counts.



(b) Representative convergence trajectory. The left Panel shows the first 100 GD gradient-norm iterations together with the full FRIDA gradient-norm trajectory. The right Panel shows the objective-value histories and the final objective values reached by both methods.

Figure 4: Comparison between Riemannian gradient descent and FRIDA on $S^2 \times S^1$. The top row summarizes performance over selected test predictors x_{test} whose global regression weights include negative values. FRIDA attains smaller best gradient norms and requires substantially fewer outer iterations than GD, while both methods obtain nearly identical final objective values. The FRIDA inner iteration counts remain well below the prescribed inner iteration budget, indicating a stable solution of the local surrogate subproblems. The bottom row shows a representative convergence trajectory: FRIDA achieves a lower gradient norm much faster than GD, and both methods converge to the same final objective value.

up to higher-order curvature terms [27, Sec. 4]. Thus, the torus experiment is a robustness study under approximate local geometry, not an exact intrinsic Fréchet regression experiment.

7.3.1 Local torus with global weights

We first study global Fréchet regression on a local patch of the embedded torus. The data are generated in angular coordinates (θ, ϕ) . We set $\theta_0 = 0, \phi_0 = \frac{\pi}{2}, R = 2.0, r = 0.7$. At the patch center, the θ -metric scale is $A_0 = R + r \cos \phi_0 = R$, which converts angular displacement in θ into local arclength. For $x_i \in [0, 1]$, the noiseless curve is chosen as a straight line in approximate orthonormal coordinates, with $L_{\text{total}} = 1.45$ and $\alpha = \pi/3$:

$$\theta(x_i) = \theta_0 + \frac{L_{\text{total}} \cos \alpha}{A_0} \left(x_i - \frac{1}{2} \right), \quad \phi(x_i) = \phi_0 + \frac{L_{\text{total}} \sin \alpha}{r} \left(x_i - \frac{1}{2} \right).$$

The responses are obtained by mapping $(\theta(x_i), \phi(x_i))$ to the embedded torus in \mathbb{R}^3 .

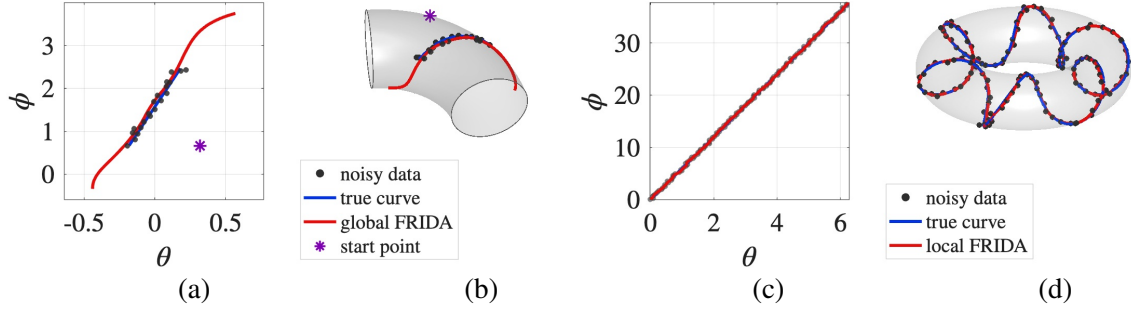


Figure 5: Fréchet regression experiments on the embedded torus. Panels (a)–(b) show global Fréchet regression on a controlled local patch: (a) gives the angular-coordinate view and (b) maps the same objects onto the local embedded torus patch in \mathbb{R}^3 . Panels (c)–(d) show local Fréchet regression along a closed curve covering the full torus: (c) gives the unwrapped angular-coordinate view and (d) shows the corresponding embedded curve in \mathbb{R}^3 . In all panels, black points denote noisy observations, blue curves denote the true trajectory, and red curves denote the DCA-based regression estimate. Purple stars mark the initialization points in panels (a)–(b). In both settings, the regression estimate closely follows the true trajectory from noisy observations.

This curve stays in a controlled local patch while crossing both positive and negative curvature regions; along it, $-0.767 \leq K(\phi) \leq 0.397$. Noisy observations are generated by

$$\theta_i^{\text{obs}} = \theta(x_i) + \frac{\sigma_{\text{intrinsic}}}{A_0} \varepsilon_i^\theta, \quad \phi_i^{\text{obs}} = \phi(x_i) + \frac{\sigma_{\text{intrinsic}}}{r} \varepsilon_i^\phi, \quad \varepsilon_i^\theta, \varepsilon_i^\phi \sim N(0, 1),$$

with $\sigma_{\text{intrinsic}} = 0.04$. This scaling makes the noise approximately isotropic under the local metric

$$ds^2 \approx A_0^2 d\theta^2 + r^2 d\phi^2.$$

The curve remains in the local normal/convexity regime described above, and the regression weights are the global affine weights.

Fig. 5(a)–(b) shows global Fréchet regression on a local patch of the embedded torus. Panel (a) gives the angular-coordinate view (θ, ϕ) , where black points denote noisy observations, the blue curve is the true response curve, the red curve is the global regression estimate, and the purple marker is the optimization start point. Panel (b) maps the same objects onto the embedded torus in \mathbb{R}^3 . The estimate closely matches the true curve within the local patch, indicating that the method accurately recovers the trajectory in this controlled setting.

7.3.2 Global torus experiment with local weights

We next consider regression on the full embedded torus, where the true response curve wraps around the entire surface. We set $R = 2.0$, $r = 0.7$, $x \in [0, 6]$, and generate the noiseless curve in angular coordinates with $\theta_0 = 0$, $\phi_0 = 0$, $N_\theta = 1$, and $N_\phi = 6$:

$$\theta(x) = \theta_0 + 2\pi N_\theta \frac{x - x_{\min}}{x_{\max} - x_{\min}}, \quad \phi(x) = \phi_0 + 2\pi N_\phi \frac{x - x_{\min}}{x_{\max} - x_{\min}}.$$

Thus, the curve winds once in the central direction and six times in the cross-sectional direction. Since it covers the full cross-sectional circle, it passes through the full curvature range of the embedded torus. For

$R = 2.0$ and $r = 0.7$, $-1.099 \leq K \leq 0.529$, so the trajectory repeatedly visits positive, zero, and negative curvature regions.

We add Gaussian noise to the unwrapped angles and then wrap modulo 2π :

$$\theta_i^{\text{obs}} = \theta(x_i) + 0.035 \varepsilon_i^\theta, \quad \phi_i^{\text{obs}} = \phi(x_i) + 0.035 \varepsilon_i^\phi, \quad \varepsilon_i^\theta, \varepsilon_i^\phi \sim N(0, 1).$$

Although the trajectory is global, each regression is computed locally. For a test point x_0 , we use observations in a local predictor window of half-width

$$\Delta x_{\text{loc}}(x_0) = 0.85 \rho_{\text{safe}} / \max\{\text{speed}(x_0), 10^{-12}\}, \quad \rho_{\text{safe}} = 0.55,$$

with $\Delta x_{\text{loc}} \in [0.04, 0.35]$, and set $h_{\text{loc}} = 0.45 \Delta x_{\text{loc}}$. Local observations are chosen using periodic distance in x , with at least 8 observations per subproblem, and normalized Gaussian weights. This keeps each local regression within an approximate intrinsic radius controlled by ρ_{safe} , so that each subproblem remains in the local normal/convexity regime described above, even though the full curve covers the entire torus.

Fig. 5(c)–(d) shows local Fréchet regression along a closed curve on the full embedded torus. Panel (c) gives the unwrapped angular-coordinate view, where the curve appears nearly linear because it winds once in θ and six times in ϕ . Black points denote noisy observations, the blue curve is the true trajectory, and the red curve is the local DCA estimate. Panel (d) maps the same curves onto the embedded torus in \mathbb{R}^3 . The close agreement between the orange and blue curves shows that the proposed method recovers the trajectory despite angular wrapping and noise.

8 Conclusions

We studied signed Fréchet regression on complete Riemannian manifolds with two-sided sectional-curvature bounds and developed FRIDA, a proximal DC framework for its computation. Since the regression weights may have mixed signs, the objective is an affine combination of squared distances and is generally non-convex, with possible nonsmoothness near cut loci. By working on strongly convex normal balls with an adaptive proximal term, we showed that the local subproblems are well posed and strongly geodesically convex. Our analysis separates the two curvature bounds: the upper bound controls convexity radii and lower Hessian bounds, while the lower bound controls Jacobi-field growth and the smoothness constants for the logarithm linearization. Under explicit signed-weight conditions, we proved the existence and interiority of minimizers, descent of the exact and inexact FRIDA iterations, stationarity of all accumulation points, and the complexity bound $O((N + 1)^{-1/2})$. In the real-analytic case, the Kurdyka–Łojasiewicz framework further gives full-sequence convergence with rates determined by the KL exponent. These results provide a theoretical foundation for FRIDA-type methods for signed Fréchet regression under local two-sided curvature control. Future work includes sharpening local rates, developing statistically consistent inexact solvers, and extending the framework to broader metric or stratified spaces where only local comparison estimates are available.

References

- [1] Bijan Afsari, Roberto Tron, and René Vidal. On the convergence of gradient descent for finding the Riemannian center of mass. *SIAM Journal on Control and Optimization*, 51(3):2230–2260, 2013.
- [2] Jason M. Altschuler, Sinho Chewi, Patrik Gerber, and Austin J. Stromme. Averaging on the Bures–Wasserstein manifold: Dimension-free convergence of gradient descent. In *Advances in Neural Information Processing Systems*, volume 34, pages 22132–22145, 2021.

- [3] Hedy Attouch and Jérôme Bolte. On the convergence of the proximal algorithm for nonsmooth functions involving analytic features. *Mathematical Programming*, 116(1):5–16, 2009.
- [4] Andrew Bennett and Nathan Kallus. The variational method of moments. *Journal of the Royal Statistical Society Series B: Statistical Methodology*, 85(3):810–841, 2023.
- [5] Ronny Bergmann, Orizon P Ferreira, Elianderson M Santos, and João Carlos O Souza. The difference of convex algorithm on Hadamard manifolds. *Journal of Optimization Theory and Applications*, 201(1):221–251, 2024.
- [6] Manfredo Perdigão do Carmo. *Riemannian geometry / Manfredo do Carmo ; translated by Francis Flaherty*. Mathematics. Theory and applications. Birkhäuser, Boston, 1992.
- [7] J. Fan and I. Gijbels. *Local polynomial modelling and its applications*, volume 66 of *Monographs on Statistics and Applied Probability*. Chapman & Hall, London, 1996.
- [8] Oisín Faust, Hamza Fawzi, and James Saunderson. A Bregman divergence view on the difference-of-convex algorithm. In *International Conference on Artificial Intelligence and Statistics*, pages 3427–3439. PMLR, 2023.
- [9] Lars Peter Hansen. Large sample properties of generalized method of moments estimators. *Econometrica: Journal of the econometric society*, pages 1029–1054, 1982.
- [10] J-B Hiriart-Urruty. Generalized differentiability/duality and optimization for problems dealing with differences of convex functions. In *Convexity and Duality in Optimization: Proceedings of the Symposium on Convexity and Duality in Optimization Held at the University of Groningen, The Netherlands June 22, 1984*, pages 37–70. Springer, 1985.
- [11] Reiner Horst and Nguyen V Thoai. DC programming: overview. *Journal of Optimization Theory and Applications*, 103:1–43, 1999.
- [12] Chang Jun Im, Jeong Min Jeon, and Byeong U Park. Local Fréchet regression with spherical predictors. *Electronic Journal of Statistics*, 19(2):5313–5367, 2025.
- [13] Robert T. Jantzen. Geodesics on the torus and other surfaces of revolution clarified using undergraduate physics tricks with bonus: Nonrelativistic and relativistic kepler problems, 2010. Lecture notes.
- [14] Krzysztof Kurdyka, Tadeusz Mostowski, and Adam Parusiński. Proof of the gradient conjecture of R. Thom. *Annals of Mathematics*, pages 763–792, 2000.
- [15] Hoai An Le Thi and Tao Pham Dinh. DC programming and DCA: thirty years of developments. *Mathematical Programming*, 169(1):5–68, 2018.
- [16] J. Lee. *Introduction to Smooth Manifolds*. Graduate Texts in Mathematics. Springer New York, 2012.
- [17] John M Lee. *Introduction to Riemannian manifolds*, volume 2. Springer, 2018.
- [18] Lu Lin and Ze Chen. A type of nonlinear Fréchet regressions. *arXiv preprint arXiv:2403.17481*, 2024.
- [19] Zhenhua Lin and Hans-Georg Müller. Total variation regularized Fréchet regression for metric-space valued data. *The Annals of Statistics*, 49(6):3510–3533, 2021.
- [20] David Martínez-Rubio, Christophe Roux, and Sebastian Pokutta. Convergence and trade-offs in Riemannian gradient descent and Riemannian proximal point. *arXiv preprint arXiv:2403.10429*, 2024.

- [21] Esfandiar Nava-Yazdani. Ridge regression for manifold-valued time-series with application to meteorological forecast. *arXiv preprint arXiv:2411.18339*, 2024.
- [22] Alexander Petersen and Hans-Georg Müller. Fréchet regression for random objects with euclidean predictors. *The Annals of Statistics*, 47(2):691–719, 2019.
- [23] Seyedehsomayeh Hosseini. Convergence of nonsmooth descent methods via Kurdyka–Lojasiewicz inequality on Riemannian manifolds. November 2015.
- [24] Asuka Takatsu. Wasserstein geometry of Gaussian measures. *Osaka Journal of Mathematics*, 48(4):1005–1026, 2011.
- [25] A Torres-Signes, MP Frías, and MD Ruiz-Medina. Multivariate manifold-valued curve regression in time. *arXiv preprint arXiv:2208.12585*, 2022.
- [26] Hoang Tuy. Global minimization of a difference of two convex functions. In *Selected Topics in Operations Research and Mathematical Economics: Proceedings of the 8th Symposium on Operations Research, Held at the University of Karlsruhe, West Germany August 22–25, 1983*, pages 98–118. Springer, 1984.
- [27] Jeff A. Viaclovsky. Math 865: Topics in Riemannian geometry. https://www.math.uci.edu/~jviaclov/courses/865_Fall_2011.pdf, 2011. Course notes.
- [28] Jeff A. Viaclovsky. Critical metrics for Riemannian curvature functionals. https://www.math.uci.edu/~jviaclov/lecturenotes/PCMI_Lectures_Final.pdf, 2013. Expanded version of IAS/PCMI lecture notes, 2013.
- [29] Melanie Weber and Suvrit Sra. On a class of geodesically convex optimization problems solved via Euclidean mm methods. *arXiv preprint arXiv:2206.11426*, 2022.
- [30] Mathijs Wintraecken. Ambient and intrinsic triangulations and topological methods in cosmology. 2015.
- [31] Chaorui Yao and Xin Jiang. A globally convergent difference-of-convex algorithmic framework and application to log-determinant optimization problems. *arXiv preprint arXiv:2306.02001*, 2023.
- [32] Yidong Zhou and Hans-Georg Müller. Network regression with graph Laplacians. *Journal of Machine Learning Research*, 23(320):1–41, 2022.
- [33] Wolfgang Ziller. Riemannian manifolds with positive sectional curvature. In *Geometry of Manifolds with Non-negative Sectional Curvature: Editors: Rafael Herrera, Luis Hernández-Lamoneda*, pages 1–19. Springer, 2014.